together with pMD2 and psPAX2 vectors in 293T cells. DMS53 was infected with the prepared viruses, and selected using puromycin at 2 ug/mL for two days.

Immunoblot analysis. Aliquots of protein were subjected to SDS/PAGE followed by immunoblot analysis using antibodies against EZH2 (#39103, Active Motif), V5 (R960-25, Invitrogen), and α-Tubulin (DM1A, Sigma) as primary antibodies, and against rabbit IgG (sc-2004, Santa Cruz, 1 : 5,000 dilution) and mouse IgG (sc-2005, Santa Cruz) as secondary antibodies. The antibodies used were well characterized previously by us and others[56]. Proteins were transferred to nitrocellulose and the resulting immunoblots were visualized using Amersham ECL Plus (GE Healthcare) and LAS-3000 (Fujifilm, Japan), and processed using MultiGauge software (Fujifilm).

Cellular immunofluorescence. Cells were washed with PBS three times and fixed with 4% paraformaldehyde for 5 min. After washed with PBS three times, cells were permeabilized with 0.2% Triton X-100 in PBS for 10 min. Introduced proteins were detected using antibodies against V5 (R960-25, Invitrogen) as primary antibody, and green-fluorescent Alexa Fluor 488 dye-labeled anti-mouse antibody (A11029, Invitrogen) as secondary antibody. Photographs were taken with Biozero BZ-8100 (KEYENCE, Osaka, Japan).

Growth curve. *JUB*- and *PTRF*-introduced DMS53 cells were seeded at density of 1×10^3 cells/well in 96-well plate, and cellular growth was analyzed using WST-8 kit (Doijndo, Japan) at 12, 36, 60, and 84 h. Cellular growth of Lu130, H209, and DMS53 with treatment by DZNep or GSK126 (Active Biochem, NJ) was also analyzed using WST-8 kit. DZNep was dissolved in PBS at 5 mM, and cells were cultured at the final concentration of 5 μM. GSK126 was dissolved in DMSO at 10 mM, and cells were cultured at 0.5, 2, and 8 μM.

Statistical analysis. Statistical analyses were performed using *t*-test and Fisher's exact test. K-means sample clustering was performed by Orange[29] (http://orange.biolab.si/citation/). Kaplan-Meier survival analysis was performed by JMP 7 (http://www.jmp.com/) and P-value was calculated by log-rank test. Survival analysis by Cox proportional-hazards regression was performed by R software (http://www.R-project.org/). In overall survival analysis, the end of follow up period was 84 months from the primary surgery and the mean follow up time of the cases was 64 months. Death as a result of SCLC was the primary end point and deaths by other causes were censored.

1. Ferlay, J. *et al.* Estimates of worldwide burden of cancer in 2008: GLOBOCAN 2008. *Int J Cancer* **127** (12), 2893–2917 (2011).
2. Read, W. L., Page, N. C., Tierney, R. M., Piccirillo, J. F. & Govindan, R. The epidemiology of bronchioloalveolar carcinoma over the past two decades: analysis of the SEER database. *Lung Cancer* **45** (2), 137–142 (2004).
3. Devesa, S. S., Bray, F., Vizcaino, A. P. & Parkin, D. M. International lung cancer trends by histologic type: male:female differences diminishing and adenocarcinoma rates rising. *Int J Cancer* **117** (2), 294–299 (2005).
4. Brownson, R. C., Chang, J. C. & Davis, J. R. Gender and histologic type variations in smoking-related risk of lung cancer. *Epidemiology* **3** (1), 61–64 (1992).
5. Otterson, G., Lin, A. & Kay, F. Genetic etiology of lung cancer. *Oncology (Williston Park)* **6** (9), 97–104, 107; discussion **108**, 111–102 (1992).
6. Sher, T., Dy, G. K. & Adjei, A. A. Small cell lung cancer. *Mayo Clin Proc* **83** (3), 355–367 (2008).
7. Gustafsson, B. I., Kidd, M., Chan, A., Malfertheiner, M. V. & Modlin, I. M. Bronchopulmonary neuroendocrine tumors. *Cancer* **113** (1), 5–21 (2008).
8. Albain, K. S., Crowley, J. J. & Livingston, R. B. Long-term survival and toxicity in small cell lung cancer. Expanded Southwest Oncology Group experience. *Chest* **99** (6), 1425–1432 (1991).
9. Lassen, U. *et al.* Long-term survival in small-cell lung cancer: posttreatment characteristics in patients surviving 5 to 18+ years--an analysis of 1,714 consecutive patients. *J Clin Oncol* **13** (5), 1215–1220 (1995).
10. Sekido, Y., Fong, K. M. & Minna, J. D. Molecular genetics of lung cancer. *Annu Rev Med* **54**, 73–87 (2003).
11. Sutherland, K. D. *et al.* Cell of origin of small cell lung cancer: inactivation of Trp53 and Rb1 in distinct cell types of adult mouse lung. *Cancer Cell* **19** (6), 754–764 (2011).
12. Pleasance, E. D. *et al.* A small-cell lung cancer genome with complex signatures of tobacco exposure. *Nature* **463** (7278), 184–190 (2010).
13. Rudin, C. M. *et al.* Comprehensive genomic analysis identifies SOX2 as a frequently amplified gene in small-cell lung cancer. *Nat Genet* **44** (10), 1111–1116 (2012).
14. Peifer, M. *et al.* Integrative genome analyses identify key somatic driver mutations of small-cell lung cancer. *Nat Genet* **44** (10), 1104–1110 (2012).
15. Bracken, A. P. & Helin, K. Polycomb group proteins: navigators of lineage pathways led astray in cancer. *Nat Rev Cancer* **9** (11), 773–784 (2009).
16. Margueron, R. & Reinberg, D. The Polycomb complex PRC2 and its mark in life. *Nature* **469** (7330), 343–349 (2011).
17. Varambally, S. *et al.* The polycomb group protein EZH2 is involved in progression of prostate cancer. *Nature* **419** (6907), 624–629 (2002).
18. Kleer, C. G. *et al.* EZH2 is a marker of aggressive breast cancer and promotes neoplastic transformation of breast epithelial cells. *Proc Natl Acad Sci U S A* **100** (20), 11606–11611 (2003).
19. Mills, A. A. Throwing the cancer switch: reciprocal roles of polycomb and trithorax proteins. *Nat Rev Cancer* **10** (10), 669–682 (2010).
20. Wilson, B. G. *et al.* Epigenetic antagonism between polycomb and SWI/SNF complexes during oncogenic transformation. *Cancer Cell* **18** (4), 316–328 (2010).
21. Kikuchi, J. *et al.* Epigenetic therapy with 3-deazaneplanocin A, an inhibitor of the histone methyltransferase EZH2, inhibits growth of non-small cell lung cancer cells. *Lung Cancer* **78** (2), 138–143 (2012).
22. Huqun *et al.* Enhancer of zeste homolog 2 is a novel prognostic biomarker in nonsmall cell lung cancer. *Cancer* **118** (6), 1599–1606 (2012).
23. Miyake, Y., Kodama, T. & Yamaguchi, K. Pro-gastrin-releasing peptide(31–98) is a specific tumor marker in patients with small cell lung carcinoma. *Cancer Res* **54** (8), 2136–2140 (1994).
24. Bhattacharjee, A. *et al.* Classification of human lung carcinomas by mRNA expression profiling reveals distinct adenocarcinoma subclasses. *Proc Natl Acad Sci U S A* **98** (24), 13790–13795 (2001).
25. Garber, M. E. *et al.* Diversity of gene expression in adenocarcinoma of the lung. *Proc Natl Acad Sci U S A* **98** (24), 13784–13789 (2001).
26. Chhatriwala, H., Jafri, N. & Salgia, R. A review of topoisomerase inhibition in lung cancer. *Cancer Biol Ther* **5** (12), 1600–1607 (2006).
27. Kirmizis, A. *et al.* Silencing of human polycomb target genes is associated with methylation of histone H3 Lys 27. *Genes Dev* **18** (13), 1592–1605 (2004).
28. Lee, T. I. *et al.* Control of developmental regulators by Polycomb in human embryonic stem cells. *Cell* **125** (2), 301–313 (2006).
29. Curk, T. *et al.* Microarray data mining with visual programming. *Bioinformatics* **21** (3), 396–398 (2005).
30. Tan, J. *et al.* Pharmacologic disruption of Polycomb-repressive complex 2-mediated gene repression selectively induces apoptosis in cancer cells. *Genes Dev* **21** (9), 1050–1063 (2007).
31. Chase, A. & Cross, N. C. Aberrations of EZH2 in cancer. *Clin Cancer Res* **17** (9), 2613–2618 (2011).
32. Zoabi, M., Sadeh, R., de Bie, P., Marquez, V. E. & Ciechanover, A. PRAJA1 is a ubiquitin ligase for the polycomb repressive complex 2 proteins. *Biochem Biophys Res Commun* **408** (3), 393–398 (2011).
33. Juan, A. H. *et al.* Polycomb EZH2 controls self-renewal and safeguards the transcriptional identity of skeletal muscle stem cells. *Genes Dev* **25** (8), 789–794 (2011).
34. Chen, H., Tu, S. W. & Hsieh, J. T. Down-regulation of human DAB2IP gene expression mediated by polycomb Ezh2 complex and histone deacetylase in prostate cancer. *J Biol Chem* **280** (23), 22437–22444 (2005).
35. Min, J. *et al.* An oncogene-tumor suppressor cascade drives metastatic prostate cancer by coordinately activating Ras and nuclear factor-kappaB. *Nat Med* **16** (3), 286–294 (2010).
36. Fan, T. *et al.* EZH2-dependent suppression of a cellular senescence phenotype in melanoma cells by inhibition of p21/CDKN1A expression. *Mol Cancer Res* **9** (4), 418–429 (2011).
37. McCabe, M. T. *et al.* EZH2 inhibition as a therapeutic strategy for lymphoma with EZH2-activating mutations. *Nature* **492** (7427), 108–112 (2012).
38. Knutson, S. K. *et al.* A selective inhibitor of EZH2 blocks H3K27 methylation and kills mutant lymphoma cells. *Nat Chem Biol* **8** (11), 890–896 (2012).
39. Hill, M. M. *et al.* PTRF-Cavin, a conserved cytoplasmic protein required for caveola formation and function. *Cell* **132** (1), 113–124 (2008).
40. Capozza, F. *et al.* Absence of caveolin-1 sensitizes mouse skin to carcinogen-induced epidermal hyperplasia and tumor formation. *Am J Pathol* **162** (6), 2029–2039 (2003).
41. Williams, T. M. *et al.* Loss of caveolin-1 gene expression accelerates the development of dysplastic mammary lesions in tumor-prone transgenic mice. *Mol Biol Cell* **14** (3), 1027–1042 (2003).
42. Volonte, D. & Galbiati, F. Polymerase I and transcript release factor (PTRF)/cavin-1 is a novel regulator of stress-induced premature senescence. *J Biol Chem* **286** (33), 28657–28661 (2011).
43. Kuang, S. Q. *et al.* Aberrant DNA methylation and epigenetic inactivation of Eph receptor tyrosine kinases and ephrin ligands in acute lymphoblastic leukemia. *Blood* **115** (12), 2412–2419 (2010).
44. Winn, R. A. *et al.* Restoration of Wnt-7a expression reverses non-small cell lung cancer cellular transformation through frizzled-9-mediated growth inhibition and promotion of cell differentiation. *J Biol Chem* **280** (20), 19625–19634 (2005).
45. O'Reilly, M. S. *et al.* Endostatin: an endogenous inhibitor of angiogenesis and tumor growth. *Cell* **88** (2), 277–285 (1997).
46. Kaneda, A., Kaminishi, M., Yanagihara, K., Sugimura, T. & Ushijima, T. Identification of silencing of nine genes in human gastric cancers. *Cancer Res* **62** (22), 6645–6650 (2002).
47. Yagi, K. *et al.* Three DNA methylation epigenotypes in human colorectal cancer. *Clin Cancer Res* **16** (1), 21–33 (2010).
48. Suehiro, T. *et al.* Thrombomodulin inhibits intrahepatic spread in human hepatocellular carcinoma. *Hepatology* **21** (5), 1285–1290 (1995).
49. Liu, P. L. *et al.* Decreased expression of thrombomodulin is correlated with tumor cell invasiveness and poor prognosis in nonsmall cell lung cancer. *Mol Carcinog* **49** (10), 874–881 (2010).
50. Marie, H. *et al.* The LIM protein Ajuba is recruited to cadherin-dependent cell junctions through an association with alpha-catenin. *J Biol Chem* **278** (2), 1220–1228 (2003).

51. Hou, Z. *et al.* The LIM protein AJUBA recruits protein arginine methyltransferase 5 to mediate SNAIL-dependent transcriptional repression. *Mol Cell Biol* **28** (10), 3198–3207 (2008).
52. Kanungo, J., Pratt, S. J., Marie, H. & Longmore, G. D. Ajuba, a cytosolic LIM protein, shuttles into the nucleus and affects embryonal cell proliferation and fate decisions. *Mol Biol Cell* **11** (10), 3299–3313 (2000).
53. Carney, D. N. *et al.* Establishment and identification of small cell lung cancer cell lines having classic and variant features. *Cancer Res* **45** (6), 2913–2923 (1985).
54. Sriuranpong, V. *et al.* Notch signaling induces rapid degradation of achaete-scute homolog 1. *Mol Cell Biol* **22** (9), 3129–3139 (2002).
55. Jiang, T. *et al.* Achaete-scute complex homologue 1 regulates tumor-initiating capacity in human small cell lung cancer. *Cancer Res* **69** (3), 845–854 (2009).
56. Kaneda, A. *et al.* Activation of Bmp2-Smad1 signal and its regulation by coordinated alteration of H3K27 trimethylation in Ras-induced senescence. *PLoS Genet* **7** (11), e1002359 (2011).
57. Zhang, Y. *et al.* Model-based analysis of ChIP-Seq (MACS). *Genome Biol* **9** (9), R137 (2008).

Acknowledgements

We thank Kaori Shiina, Hiroko Meguro and Kyoko Fujinaka for their technical assistance. This work was supported in part by Grants-in-Aid for Scientific Research from the Ministry of Education, Culture, Sports, Science and Technology of Japan, the NFAT project from the New Energy and Industrial Technology Development Organization (NEDO), by JST Core Research for Evolutional Science and Technology (CREST) program, and by the Intramural Research Program of the NIH, National Cancer Institute, Center for Cancer Research.

Author contributions

T.S. performed experiments, generated data and figures and co-wrote the manuscript. A.K. designed study, supervised the study, performed experiments, generated data and figures and co-wrote the manuscript. S.T. analysed data and generated figures. T.I. performed experiments. S.Y. analysed data. T.F. analysed data. R.Y. analysed data. Y.T. performed experiments. T.N. supervised the study. V.E.M. performed experiments. Y.I. collected clinical samples and information. M.I. supervised data. H.A. designed study and supervised the study.

Additional information

Supplementary information accompanies this paper at http://www.nature.com/scientificreports

Competing financial interests: The authors declare no competing financial interests.

How to cite this article: Sato, T. *et al.* PRC2 overexpression and PRC2-target gene repression relating to poorer prognosis in small cell lung cancer. *Sci. Rep.* 3, 1911; DOI:10.1038/srep01911 (2013).

LETTER

doi:10.1038/nature12347

Obesity-induced gut microbial metabolite promotes liver cancer through senescence secretome

Shin Yoshimoto[1,2]*, Tze Mun Loo[1,2,3], Koji Atarashi[4,5], Hiroaki Kanda[6], Seidai Sato[1,2], Seiichi Oyadomari[7], Yoichiro Iwakura[8], Kenshiro Oshima[9], Hidetoshi Morita[10], Masahira Hattori[9], Kenya Honda[2,4], Yuichi Ishikawa[6], Eiji Hara[1,2] & Naoko Ohtani[1,5]*

Obesity has become more prevalent in most developed countries over the past few decades, and is increasingly recognized as a major risk factor for several common types of cancer[1]. As the worldwide obesity epidemic has shown no signs of abating[2], better understanding of the mechanisms underlying obesity-associated cancer is urgently needed. Although several events were proposed to be involved in obesity-associated cancer[1,3], the exact molecular mechanisms that integrate these events have remained largely unclear. Here we show that senescence-associated secretory phenotype (SASP)[4,5] has crucial roles in promoting obesity-associated hepatocellular carcinoma (HCC) development in mice. Dietary or genetic obesity induces alterations of gut microbiota, thereby increasing the levels of deoxycholic acid (DCA), a gut bacterial metabolite known to cause DNA damage[6]. The enterohepatic circulation of DCA provokes SASP phenotype in hepatic stellate cells (HSCs)[7], which in turn secretes various inflammatory and tumour-promoting factors in the liver, thus facilitating HCC development in mice after exposure to chemical carcinogen. Notably, blocking DCA production or reducing gut bacteria efficiently prevents HCC development in obese mice. Similar results were also observed in mice lacking an SASP inducer[8] or depleted of senescent HSCs, indicating that the DCA–SASP axis in HSCs has key roles in obesity-associated HCC development. Moreover, signs of SASP were also observed in the HSCs in the area of HCC arising in patients with non-alcoholic steatohepatitis[3], indicating that a similar pathway may contribute to at least certain aspects of obesity-associated HCC development in humans as well. These findings provide valuable new insights into the development of obesity-associated cancer and open up new possibilities for its control.

Cellular senescence is a process occurring in normal cells in response to telomere erosion or oncogene activation, acting through checkpoint activation and stable cell-cycle arrest as a barrier to tumorigenesis[9,10]. Recent studies, however, reveal that senescent cells also develop a secretory profile composed mainly of inflammatory cytokines, chemokines and proteases, a typical signature termed the senescence-associated secretory phenotype (SASP)[4] or the senescence messaging secretome (SMS)[5], hereafter referred to as SASP. Some of the SASP factors have cell-autonomous activities that reinforce senescence cell-cycle arrest[5] and/or promote clearance of senescent cells[11,12], but other SASP factors have cell non-autonomous functions associated with inflammation and tumorigenesis promotion[4], indicating that SASP contributes positively and negatively to cancer development, depending on the biological context[4,5]. Because some of the SASP factors, such as IL-6 and PAI-1[4,5], are known to increase cancer risk in obesity[1,13], we propose that SASP may contribute to obesity-associated cancer.

To explore this possibility, we first set up a system to examine the impact of dietary obesity on tumorigenesis, using wild-type C57BL/6 mice. However, we were unable to detect a statistically significant difference in cancer development between obese mice fed a high-fat diet (HFD) and lean mice fed a normal diet (data not shown), implying that a certain level of oncogenic stimuli might be required for obesity-associated cancer, especially in wild-type mice maintained in a specific pathogen free (SPF) environment. Because the Ras-pathway is frequently activated in human cancers, including hepatocellular carcinoma (HCC)[14], we decided to use a treatment with DMBA (7,12-dimethylbenz(*a*)anthracene, a chemical carcinogen that causes an oncogenic Ras mutation) at the neonatal stage, a protocol known to generate a variety of tumours throughout the body[15]. In this setting, we also took advantage of using p21-*p*-luc mice, in which the expression of the $p21^{Waf1/Cip1}$ gene (a senescence inducer, also known as *Cdkn1a*) can be monitored noninvasively using a bioluminescence imaging (BLI) technique[16]. The neonatal p21-*p*-luc mice were therefore treated with a single application of DMBA, followed by feeding either HFD or normal diet for 30 weeks (Fig. 1a). Interestingly, a marked increase of the bioluminescent signal was observed in the abdomen of the obese mice, and it originated mainly from liver cancer (Supplementary Fig. 1). Notably, all HFD-fed mice developed HCC, whereas only 5% of -mice fed normal diet developed malignant tumours in lung, but not liver (Fig. 1b–e and Supplementary Fig. 2). Importantly, moreover, similar HCC development was also observed when genetically obese (*ob/ob*, also known as $Lep^{ob/ob}$) mice were treated with DMBA at the neonatal stage (Supplementary Fig. 3a–d), indicating that obesity, but not the HFD, promotes HCC development.

Because the induction of $p21^{Waf1/Cip1}$ expression was observed in liver, particularly in the area of liver cancer (Supplementary Fig. 1c), we speculated that senescent cells might be present in the vicinity of cancerous hepatocytes. Indeed, $p21^{Waf1/Cip1}$ expression was observed only in activated hepatic stellate cells (HSCs), which express α-smooth muscle actin (α-SMA) and desmin[7] (Fig. 1f). Furthermore, a number of other senescence markers[9,10], such as $p16^{INK4a}$ expression, signs of DNA damage (53BP1 foci and γH2AX foci) and inhibited cell proliferation (the absence of bromodeoxyuridine incorporation and Ki-67 expression), were also observed in activated HSCs despite absence of oncogenic *ras* mutation (Fig. 1f and Supplementary Figs 3e and 4). Interestingly, moreover, increased expression of IL-6, Gro-α, CXCL9 (major components of SASP)[4,5], but not HGF (a differentiation marker)[7], was observed in activated HSCs, but not in other types of liver cells (Fig. 1f and Supplementary Figs 3e and 5), indicating that these activated HSCs are senescing and may promote obesity-associated HCC development via SASP. It should be noted that, unlike the study using carbon tetrachloride (CCl_4)[11], fibrosis was not apparent in HFD-fed mice (Supplementary Fig. 6), precluding the possibility that the appearance of senescent HSCs was a by-product of liver fibrosis.

[1]Division of Cancer Biology, Cancer Institute, Japanese Foundation for Cancer Research, Koto-ku, Tokyo 135-8550, Japan. [2]CREST, Japan Science and Technology Agency, Kawaguchi, Saitama 332-0012, Japan. [3]Department of Applied Biological Science, Tokyo University of Science, Noda, Chiba 278-8510, Japan. [4]Research Center for Allergy and Immunology, RIKEN, Yokohama, Kanagawa 230-0045, Japan. [5]PRESTO, Japan Science and Technology Agency, Kawaguchi, Saitama 332-0012, Japan. [6]Division of Pathology, Cancer Institute, Japanese Foundation for Cancer Research, Koto-ku, Tokyo 135-8550, Japan. [7]Institute for Genome Research, University of Tokushima, Tokushima 770-8503, Japan. [8]Research Institute for Biological Science, Tokyo University of Science, Noda, Chiba 278-8510, Japan. [9]Graduate School of Frontier Sciences, University of Tokyo, Kashiwa, Chiba 277-8561, Japan. [10]School of Veterinary Medicine, Azabu University, Sagamihara, Kanagawa 229-8501, Japan.
*These authors contributed equally to this work.

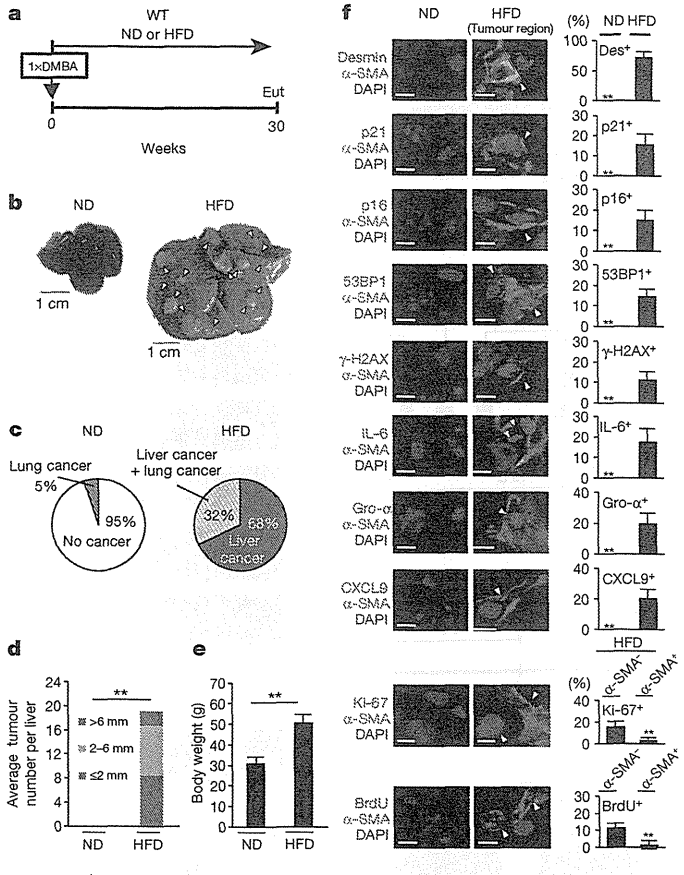

Figure 1 | Cellular senescence in HSCs. **a**, Timeline of the experimental procedure ($n = 19$ per group). Eut, euthanasia; ND, normal diet. **b**, Representative macroscopic photographs of livers. Arrowheads indicate HCCs. **c**, The ratios of cancer formation. **d**, The average liver tumour numbers and their relative size distribution. **e**, The average body weights at the age of 30 weeks. **f**, Immunofluorescence analysis of liver section. HSCs were visualized by α-SMA staining and DNA was stained by 4′,6-diamidino-2-phenylindole (DAPI). Scale bars, 2.5 μm. Arrowheads indicate α-SMA expressing cells that were positive for indicated markers. The histograms indicate the percentages of α-SMA-expressing cells that were positive for indicated markers. At least 100 cells were scored per group. For all graphs, error bars indicate mean ± standard deviation (s.d.). $^{**}P < 0.01$.

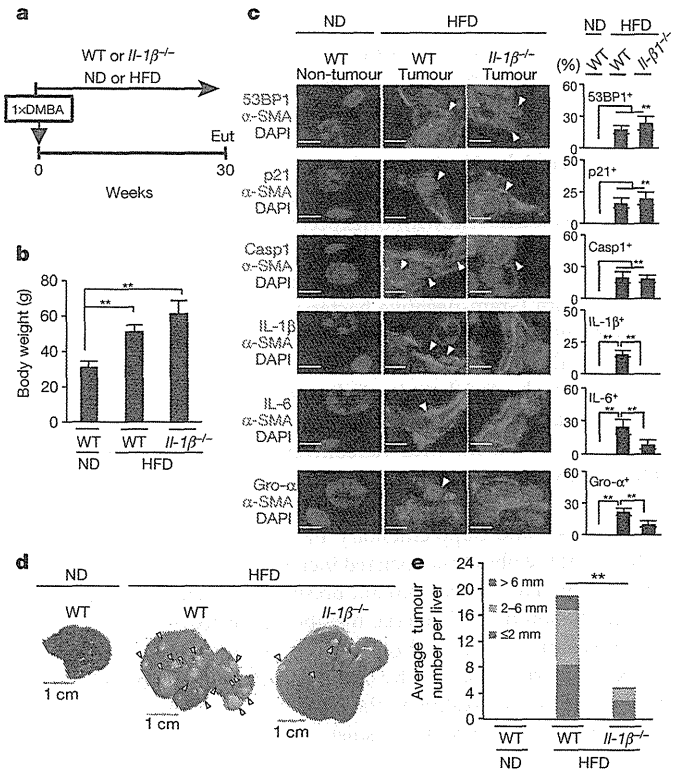

Figure 2 | IL-1β deficiency alleviates obesity-induced HCC development. **a**, Timeline of the experimental procedure (wild type (WT), $n = 19$; *Il-1β*$^{-/-}$, $n = 9$). **b**, The average body weights at the age of 30 weeks. **c**, Immunofluorescence analysis of liver sections. HSCs were visualized by α-SMA staining and DNA was stained by DAPI. Scale bars, 2.5 μm. The histograms indicate the percentages of α-SMA-expressing cells that were positive for indicated markers. At least 100 cells were scored per group. **d**, Representative macroscopic photographs of livers. Arrowheads indicate HCCs. **e**, The average liver tumour numbers and their relative size distribution. For all graphs, error bars indicate mean ± s.d. $^{**}P < 0.01$.

To ascertain the role of SASP in obesity-associated HCC development, we next sought evidence that the blockage of SASP can reduce obesity-associated HCC development. Although we were unable to detect the expression of IL-1α (an upstream regulator of SASP induction)[8] in HSCs, significant induction of IL-1β (a functional homologue of IL-1α) and its activator, caspase-1 (an essential component of the inflammasome), was observed in senescent HSCs (Fig. 2a–c). Moreover, the addition of recombinant IL-1β caused the dose-dependent induction of *Il-6* and *Gro-α* (also known as *Cxcl1*) gene expression in cultured primary murine HSCs (Supplementary Fig. 7a), indicating that inflammasome activation and subsequent IL-1β maturation can act as an upstream regulator of SASP induction in HSCs. Indeed, the levels of SASP factor expression in activated HSCs were substantially diminished in mice lacking the *Il-1β* gene (*Il-1β*$^{-/-}$ mice, also known as *Il1b*$^{-/-}$) (Fig. 2c), and the numbers and sizes of the liver tumours that developed in *Il-1β*$^{-/-}$ mice were strikingly reduced, as compared with wild-type mice (Fig. 2d, e), although the degree of steatohepatitis was not attenuated (Supplementary Fig. 8a, b). It should be noted, however, that other senescence markers, such as 53BP1 foci, p21$^{Waf1/Cip1}$ expression and inhibited cell proliferation, were still observed in the activated HSCs of *Il-1β*$^{-/-}$ mice (Fig. 2c and Supplementary Fig. 8c). These results are somewhat consistent with a recent observation that the expression of p21$^{Waf1/Cip1}$ can induce senescence cell-cycle arrest without SASP induction[17], suggesting that SASP, but not senescence cell-cycle arrest, promotes obesity-associated HCC development.

To further verify this idea, we next attempted to deplete senescent HSCs from obese wild-type mice treated with DMBA at the neonatal stage. As reported previously[18], an intravenous injection of liposomes carrying small interfering RNA (siRNA) against HSP47 substantially reduced the abundance of activated HSCs, coinciding with a significant reduction of HCC development (Supplementary Fig. 9a–f). Note that this was not accompanied by an attenuation of steatohepatitis (Supplementary Fig. 9g, h). These results, along with the data from *Il-1β*$^{-/-}$ mice (Fig. 2), strongly indicate that senescent HSCs have enhancing roles in HCC development via SASP, at least in the neonatal DMBA plus obesity-induced HCC model. It is also noteworthy that neither the deletion of the *Il-1β* gene nor the depletion of senescent HSCs caused appreciable weight loss (Fig. 2b and Supplementary Fig. 9c), implying that there may be an indirect link between obesity and HCC development, at least in this experimental setting. These observations then raised the question of how obesity provokes SASP in HSCs.

Emerging evidence has indicated that alterations of intestinal microbiota are associated with obesity[19]. Furthermore, the activation of toll-like receptor (TLR) 4 by lipopolysaccharide (LPS) from intestinal Gram-negative bacteria has been shown to promote HCC development, in an HCC model using DEN (diethyl nitrosamine) plus CCl_4 treatment[20]. We thus explored the possibility that intestinal bacteria have key roles in obesity-associated HCC development. Indeed, a

treatment with a well-established oral antibiotic cocktail (4Abx), which reduces the number of commensal intestinal bacteria[20], caused a marked reduction of HCC development, accompanied by a marked decrease in senescent HSCs in the neonatal DMBA plus obesity-induced HCC model (Fig. 3 and Supplementary Fig. 3). As reported[20], 4Abx treatment resulted in not only a > 99.5% reduction of the presence of bacterial 16S ribosomal RNA gene in faeces, but also an enlargement of caecum commonly observed in germ-free mice (Fig. 3b and data not shown). Unexpectedly, however, a slight increase, rather than decrease, in HCC development was observed in mice lacking the *Tlr4* gene ($Tlr4^{-/-}$) (Supplementary Fig. 10), indicating that LPS from Gram-negative bacteria is unlikely to promote HCC development in this setting. Indeed, meta 16S rRNA gene sequencing analysis of the intestinal microbiota revealed that the percentage of Gram-positive bacterial strains indigenous to the human and rodent intestinal tracts[6] was dramatically increased with a HFD (Fig. 4a). Moreover, a treatment with vancomycin (VCM), an antibiotic that preferentially targets Gram-positive bacteria, alone was sufficient to block HCC development and the appearance of senescent HSCs (Figs 3d–f, 4a and Supplementary Fig. 3). These results lead us to propose that the obesity-associated increase of Gram-positive bacteria may promote HCC development, presumably through the enterohepatic circulation of gut bacterial metabolites or toxins.

To substantiate this idea, the serum metabolites of HFD- and normal-diet-fed mice were analysed by liquid chromatography mass spectrometry (LC-MS). Interestingly, the level of deoxycholic acid (DCA), a secondary bile acid produced solely by the 7α-dehydroxylation of primary bile acids carried out by gut bacteria such as strains belonging to *Clostridium* cluster XI and XIVa[6] (VCM-sensitive Gram-positive bacteria), was substantially increased by the HFD feeding, and was reduced by antibiotic treatments (Figs 3a and 4b). Note that DCA is known to cause DNA damage through reactive oxygen species production[21] and DNA damage is a critical inducer of SASP[4,22]. Moreover, in addition to colon carcinogenesis[23], DCA has been shown to enhance liver carcinogenesis[24]. These notions prompted us to examine if DCA has key roles in obesity-associated HCC development. To this end, we attempted to lower the levels of DCA, by either decreasing the 7α-dehydroxylation activity with difructose anhydride III (DFA III)[25] or stimulating bile acid secretion with ursodeoxycholic acid (UDCA)[26]. Notably, lowering the DCA concentration substantially reduced HCC development, accompanied by a marked decrease in senescent HSCs in obese mice treated with DMBA at the neonatal stage (Fig. 4b and

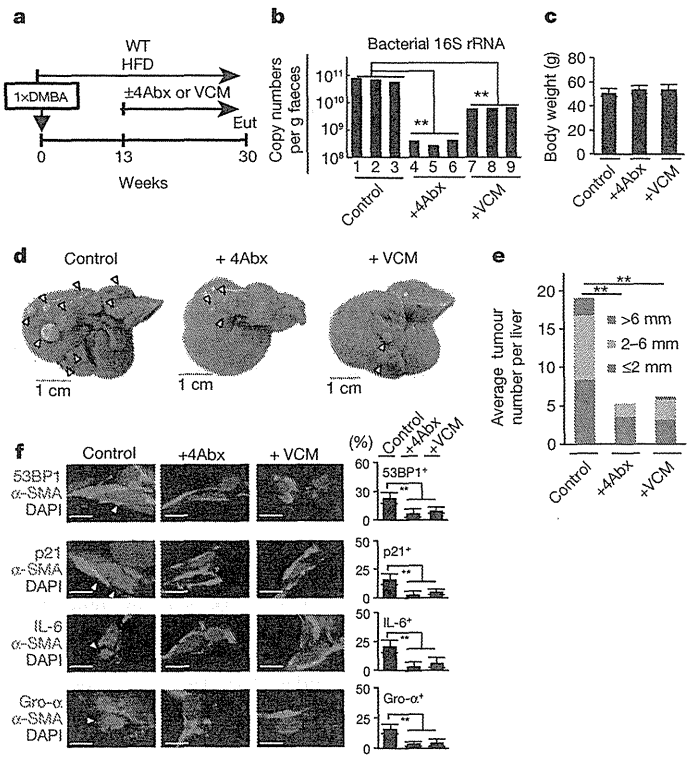

Figure 3 | Antibiotics treatments alleviate obesity-induced HCC development. **a**, Timeline of the experimental procedure (HFD, $n = 19$; HFD+4Abx, $n = 12$; HFD+VCM, $n = 6$). **b**, The copy number of intestinal bacteria in faeces of indicated mice. **c**, The average body weights at the age of 30 weeks. **d**, Representative macroscopic photograph of livers. Arrowheads indicate HCCs. **e**, The average tumour numbers and their relative size distribution. **f**, Immunofluorescence analysis of liver sections. HSCs were visualized by α-SMA staining and DNA was stained by DAPI. Scale bars, 2.5 μm. The histograms indicate the percentages of α-SMA expressing cells that were positive for indicated markers. At least 200 cells were scored per group. For all graphs, error bars indicate mean ± s.d. $^{**}P < 0.01$.

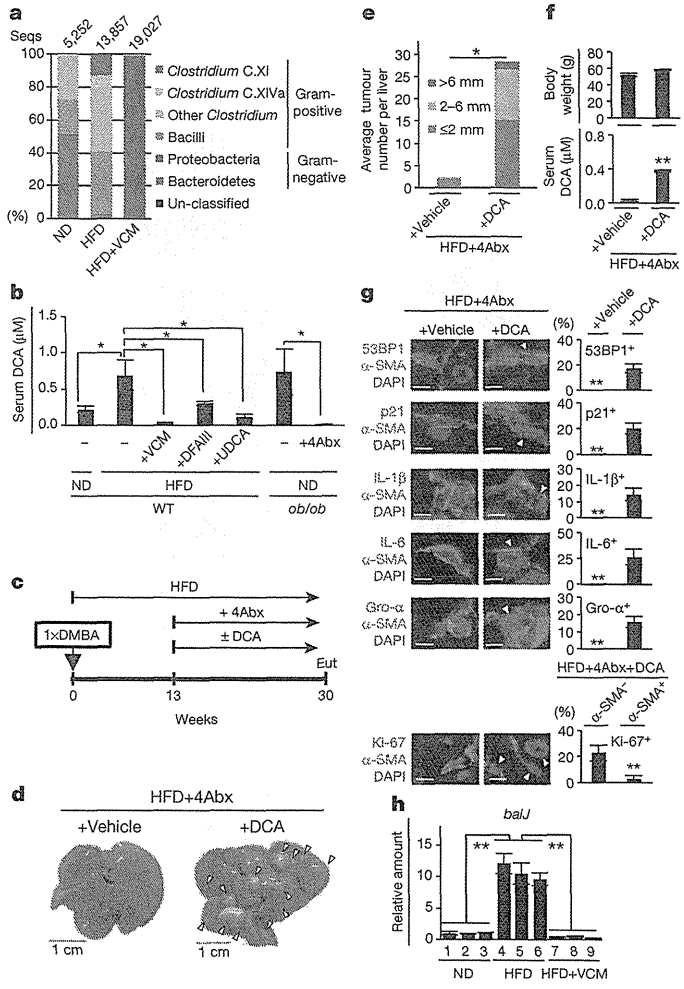

Figure 4 | Bacterial metabolite promotes obesity-induced HCC development. **a**, The relative abundance of OTUs (%) in the faecal bacterial community. Data are representative of five mice per group. **b**, Serum DCA concentration (ND, $n = 4$; HFD, $n = 6$; HFD+VCM, $n = 3$; HFD+DFAIII, $n = 3$; HFD+UDCA, $n = 3$; *ob/ob*, $n = 3$; *ob/ob*+4Abx, $n = 3$). Error bars indicate mean ± s.e.m. **c**, Timeline of the experimental procedure ($n = 3$ per group). **d**, Representative macroscopic photographs of livers. Arrowheads indicate HCCs. **e**, The average tumour numbers and their relative size distribution. **f**, The average body weight and serum DCA concentration. **g**, Immunofluorescence analysis of liver sections. Scale bars, 2.5 μm. The histograms indicate the percentages of α-SMA-expressing cells that were positive for indicated markers. At least 100 cells were scored per group. **h**, The quantitative real time PCR (qPCR) analysis of *baiJ* gene in the faeces (180 mg) of indicated mice used in **a**. For all graphs except **b**, error bars indicate mean ± s.d. $^{*}P < 0.05$, $^{**}P < 0.01$.

Supplementary Figs 11 and 12). In a reciprocal set of experiments, we also assessed whether DCA-feeding enhances HCC development in mice treated with DMBA at the neonatal stage (Fig. 4c). Intriguingly, although DCA feeding alone was insufficient to enhance HCC development in lean mice fed a normal diet at 30 weeks (data not shown), a significant enhancement of HCC development (Fig. 4c–f), accompanied by the appearance of senescence cell-cycle arrest and SASP in HSCs (Fig. 4g), was observed when HFD-fed mice treated with 4Abx were fed DCA for 17 weeks.

Notably, operational taxonomic unit (OTU)-based bacterial diversity analysis (Fig. 4a), in conjunction with a quantitative PCR analysis (Supplementary Fig. 13), revealed that the population of cluster XI of the genus *Clostridium* was strikingly increased in HFD-fed mice. Interestingly, phylogenetic analysis of the bacterial OTUs revealed that the population of *Clostridium* cluster XI is composed of a single bacterial taxon (OTU-1105) close to the DCA-producing strain *Clostridium sordellii*, and represents more than 12% of the faecal bacteria in HFD-fed mice (Supplementary Fig. 14). Concordantly, moreover, the abundance of the *baiJ* gene, a gene involved in bile acid 7α-dehydroxylation[27], was remarkably increased in faeces of mice fed HFD and was reduced by VCM treatment (Fig. 4h). On the other hand, a bacterial taxon (OTU-154) close to other DCA producing strains belonging to *Clostridium* cluster XIVa (*Clostridium hylemonae* and *Clostridium scindens*) represents only 0.5% of the total faecal bacteria in HFD-fed mice (Supplementary Fig. 14). Thus, although other bacteria may also be involved here, the simplest explanation for our data is that OTU-1105 belonging to *Clostridium* cluster XI contribute to an increase in the DCA level at least to some extent in HFD-fed mice.

Finally, to further support and extend our murine data to human biology, we tested whether IL-1β treatment can induce SASP in cultured primary human HSCs. As in murine HSCs, the addition of recombinant IL-1β caused the induction of *Il-6* and *Il-8* (a functional homologue of murine *Gro-α*) gene expression in cultured primary human HSCs (Supplementary Fig. 7b). Importantly, moreover, signs of cellular senescence and SASP were also observed in the HSCs without serious fibrosis in the area of HCC arising in patients with non-alcoholic steatohepatitis (NASH)[3] (8 out of 26) (Supplementary Fig. 15). This is somewhat consistent with previous observations that replicative senescence of cultured human HSCs is accompanied by a pronounced inflammatory but less fibrogenic phenotype[28] and a certain percentage of NASH- associated HCC arose from the non-cirrhotic liver[29]. Unlike rodents, the human liver cannot 7α-hydroxylate DCA, forming cholic acid[6]. Hence, DCA can accumulate to very high levels (>50%) in the bile acid pool of humans[6]. These data, together with the previous observation that high fat consumption resulted in higher faecal DCA concentrations in healthy male volunteers (ages 20-60)[30], suggest that DCA-induced senescent HSCs may contribute to at least certain aspects of obesity-associated HCC development via SASP in humans as well.

It should be noted that although many of the perturbations, for example, the *Il-1β* knockout, antibiotics treatment and lower DCA levels, significantly prevent HCC development, residual HCCs were still observed with these perturbations (Figs 2e and 3e and Supplementary Figs 11c and 12c). These results, in conjunction with the observation that DCA-feeding alone was insufficient to enhance HCC development in lean mice fed a normal diet until at least 30 weeks (data not shown), imply that an additional factor associated with obesity may exist to promote obesity-associated HCC development. Nevertheless, combining published data[14,19,21,24,30] with our findings, it is clear that the increased levels of DCA produced by gut bacteria play key roles in the promotion of obesity-associated HCC development via provoking SASP in HSCs, at least in the neonatal DMBA plus obesity-induced HCC model (Supplementary Fig. 16). A greater understanding of the molecular mechanisms linking gut microbial metabolite to SASP will therefore provide valuable new insights into how to bypass this undesirable side effect of cellular senescence.

METHODS SUMMARY

Chemically-induced carcinogenesis. DMBA treatments[15] consisted of a single application of 50 μl of a solution 0.5% DMBA (7,12-dimethylbenz [*a*]anthracene, Sigma) in acetone to the dorsal surface on postnatal day 4–5. Mother mice with pups were then fed either normal diet or HFD until weaning. At the age of 4 weeks old, pups were weaned and continuously fed either normal diet or HFD until euthanized.

Bacterial 16S rRNA amplicon sequencing and analysis. Bacterial genomic DNA was isolated from mice faeces, amplified for V1–V4 hypervariable regions of the 16S rRNA gene, and used for pyrosequencing analysis.

Full Methods and any associated references are available in the online version of the paper.

Received 10 December 2012; accepted 4 June 2013.
Published online 26 June 2013.

1. Khandekar, M. J., Cohen, P. & Spiegelman, B. M. Molecular mechanisms of cancer development in obesity. *Nature Rev. Cancer* **11,** 886–895 (2011).
2. Calle, E. E. & Kaaks, R. Overweight, obesity and cancer: epidemiological evidence and proposed mechanisms. *Nature Rev. Cancer* **4,** 579–591 (2004).
3. Sun, B. & Karin, M. Obesity, inflammation, and liver cancer. *J. Hepatol.* **56,** 704–713 (2012).
4. Coppé, J. P. *et al.* Senescence-associated secretory phenotypes reveal cell-nonautonomous functions of oncogenic RAS and the p53 tumor suppressor. *PLoS Biol.* **6,** 2853–2868 (2008).
5. Kuilman, T. & Peeper, D. S. Senescence-messaging secretome: SMS-ing cellular stress. *Nature Rev. Cancer* **9,** 81–94 (2009).
6. Ridlon, J. M., Kang, D. J. & Hylemon, P. B. Bile salt biotransformations by human intestinal bacteria. *J. Lipid Res.* **47,** 241–259 (2006).
7. Friedman, S. L. Hepatic stellate cells: protean, multifunctional, and enigmatic cells of the liver. *Physiol. Rev.* **88,** 125–172 (2008).
8. Orjalo, A. V., Bhaumik, D., Gengler, B. K., Scott, G. K. & Campisi, J. Cell surface-bound IL-1α is an upstream regulator of the senescence-associated IL-6/IL-8 cytokine network. *Proc. Natl Acad. Sci. USA* **106,** 17031–17036 (2009).
9. Collado, M. & Serrano, M. Senescence in tumours: evidence from mice and humans. *Nature Rev. Cancer* **10,** 51–57 (2010).
10. Kuilman, T., Michaloglou, C., Mooi, W. J. & Peeper, D. S. The essence of senescence. *Genes Dev.* **24,** 2463–2479 (2010).
11. Krizhanovsky, V. *et al.* Senescence of activated stellate cells limits liver fibrosis. *Cell* **134,** 657–667 (2008).
12. Kang, T. W. *et al.* Senescence surveillance of pre-malignant hepatocytes limits liver cancer development. *Nature* **479,** 547–551 (2011).
13. Park, E. J. *et al.* Dietary and genetic obesity promote liver inflammation and tumorigenesis by enhancing IL-6 and TNF expression. *Cell* **140,** 197–208 (2010).
14. Newell, P. *et al.* Ras pathway activation in hepatocellular carcinoma and anti-tumoral effect of combined sorafenib and rapamycin *in vivo*. *J. Hepatol.* **51,** 725–733 (2009).
15. Serrano, M. *et al.* Role of the *INK4a* locus in tumor suppression and cell mortality. *Cell* **85,** 27–37 (1996).
16. Ohtani, N. *et al.* Visualizing the dynamics of $p21^{Waf1/Cip1}$ cyclin-dependent kinase inhibitor expression in living animals. *Proc. Natl Acad. Sci. USA* **104,** 15034–15039 (2007).
17. Coppé, J.-P. *et al.* Tumor suppressor and aging biomarker $p16^{INK4a}$ induces cellular senescence without the associated inflammatory secretory phenotype. *J. Biol. Chem.* **286,** 36396–36403 (2011).
18. Sato, Y. *et al.* Resolution of liver cirrhosis using vitamin A-coupled liposomes to deliver siRNA against a collagen-specific chaperone. *Nature Biotechnol.* **26,** 431–442 (2008).
19. Ley, R. E., Turnbaugh, P. J., Klein, S. & Gordon, J. I. Microbial ecology: human gut microbes associated with obesity. *Nature* **444,** 1022–1023 (2006).
20. Dapito, D. H. *et al.* Promotion of hepatocellular carcinoma by the intestinal microbiota and TLR4. *Cancer Cell* **21,** 504–516 (2012).
21. Payne, C. M. *et al.* Deoxycholate induces mitochondrial oxidative stress and activates NF-κB through multiple mechanisms in HCT-116 colon epithelial cells. *Carcinogenesis* **28,** 215–222 (2007).
22. Takahashi, A. *et al.* DNA damage signaling triggers degradation of histone methyltransferases through APC/C^{Cdh1} in senescent cells. *Mol. Cell* **45,** 123–131 (2012).
23. McGarr, S. E., Ridlon, J. M. & Hylemon, P. B. Diet, anaerobic bacterial metabolism, and colon cancer: a review of the literature. *J. Clin. Gastroenterol.* **39,** 98–109 (2005).
24. Kitazawa, S. *et al.* Enhanced preneoplastic liver lesion development under 'selection pressure' conditions after administration of deoxycholic or lithocholic acid in the initiation phase in rats. *Carcinogenesis* **11,** 1323–1328 (1990).
25. Minamida, K., Ohashi, M., Hara, H., Asano, K. & Tomita, F. Effects of ingestion of difructose anhydride III (DFA III) and the DFA III-assimilating bacterium *Ruminococcus productus* on rat intestine. *Biosci. Biotechnol. Biochem.* **70,** 332–339 (2006).
26. Beuers, U. Drug insight: mechanisms and sites of action of ursodeoxycholic acid in cholestasis. *Nat. Clin. Pract. Gastroenterol. Hepatol.* **3,** 318–328 (2006).
27. Ridlon, J. M. & Hylemon, P. B. Identification and characterization of two bile acid coenzyme A transferases from *Clostridium scindens*, a bile acid 7α-dehydroxylating intestinal bacterium. *J. Lipid Res.* **53,** 66–76 (2012).

28. Schnabl, B., Purbeck, G. A., Choi, Y. H., Hagedorn, C. H. & Brenner, D. A. Replicative senescence of activated human hepatic stellate cells is accompanied by a pronounced inflammatory but less fibrogenic phenotype. *Hepatology* **37,** 653–664 (2003).
29. Takuma, Y. & Nouso, K. Nonalcoholic steatohepatitis-associated hepatocellular carcinoma: our case series and literature review. *World J. Gastroenterol.* **16,** 1436–1441 (2010).
30. Rafter, J. J. *et al.* Cellular toxicity of fecal water depends on diet. *Am. J. Clin. Nutr.* **45,** 559–563 (1987).

Supplementary Information is available in the online version of the paper.

Acknowledgements The authors thank M. Oshima for suggestions in antibiotics treatment and members of the Hara laboratory for discussion during the preparation of this manuscript. This work was supported by grants from Japan Science and Technology Agency (JST), Ministry of Education, Culture, Sports, Science and Technology of Japan (MEXT), Ministry of Health, Labour and Welfare of Japan (MHLW), Uehara Memorial Foundation and Takeda Science Foundation. S.Y. was partly supported by a postdoctoral fellowship from the Japan Society for Promotion of Science (JSPS). T.M.L. was partly supported by an international scholarship from the Ajinomoto Scholarship Foundation.

Author Contributions E.H. and N.O. designed the experiments, analysed the data and wrote the manuscript. N.O., S.Y. and T.M.L. performed obesity-induced liver cancer experiments. K.A., K.O., H.M., M.H. and K.H. performed bacterial genome data analysis. H.K., S.S. and Y.I. performed histopathological analysis of mouse and human liver cancer specimens. S.O. performed metabolite analysis. Y.I. provided *Il-1β*$^{-/-}$ mice. E.H. oversaw the projects.

Author Information Bacterial 16S rRNA amplicon sequence data have been deposited in DDBJ (http://www.ddbj.nig.ac.jp/index-e.html) with the accession number DRA000952. Reprints and permissions information is available at www.nature.com/reprints. The authors declare no competing financial interests. Readers are welcome to comment on the online version of the paper. Correspondence and requests for materials should be addressed to E.H. (eiji.hara@jfcr.or.jp).

METHODS

Mice and diet. The *p21-p-luc* mice (CD1)[16] were backcrossed with C57BL/6 mice for eight generations. The leptin-deficient (*ob/ob*) mice (C57BL/6) were purchased from Charles River Laboratories Japan, Inc. *Tlr4*$^{-/-}$ mice (C57BL/6) were purchased from Oriental Bioservices. *Il-1β*$^{-/-}$ mice (C57BL/6) were provided by Y. Iwakura[31]. Male mice were used for all the experiments in this study. The mice were maintained under specific pathogen-free (SPF) conditions, on a 12-h light-dark cycle, and fed normal diet (CE-2 from CLEA Japan Inc., composed of 12 kcal% fat, 29 kcal% protein, 59 kcal% carbohydrates) or high-fat diet (HFD, D12492 from Research Diets Inc., composed of 60 kcal% fat, 20 kcal% protein, 20 kcal% carbohydrates) *ad libitum*. Mice with more than 45 g weight at the age of 30 weeks old were used as obese mice for all the experiments. We measured the amount of food our mice eat and found that a 50 g HFD mouse eats 3.44 g food a day. This equates to 1.2 g of fat per day or 24 g per kg. According to the Reagan-Shaw equation[32] (human equivalent dose (mg kg^{-1}) = mouse dose (mg kg^{-1}) × mouse K_m factor ÷ human K_m factor; where the mouse and human K_m factors are 3 and 37, respectively), this is equivalent to a 70 kg human eating 136 g of fat a day. The sample size used in this study was determined based on the expense of data collection, and the need to have sufficient statistical power. Randomization and blinding were not used in this study. All animal experiments were cared for by protocols approved by the Committee for the Use and Care of Experimental Animals of the Japanese Foundation for Cancer Research (JFCR).

Chemically induced carcinogenesis. DMBA treatments[15] consisted of a single application of 50 μl of a solution 0.5% DMBA (7,12-dimethylbenz(*a*)anthracene, Sigma) in acetone to the dorsal surface on postnatal day 4–5. After this application, mother mice with pups were fed normal diet or HFD. At the age of 4 weeks old, pups were weaned and continuously fed either normal diet or HFD until euthanized. Evaluation of tumour number and size was determined by counting the number of visible tumours and measuring the size of the tumour.

Bioluminescence imaging. Bioluminescence imaging was performed as previously described[16,33]. In brief, for the detection of luciferase expression, mice were anesthetized, injected intraperitoneally with D-luciferin sodium salt (75 mg kg^{-1}) 5 min before beginning photon recording. Mice were placed in the light-tight chamber and a grey-scale image of the mice was first recorded with dimmed light followed by acquisition of luminescence image using a cooled charged-coupled device (CCD) camera (PIXIS 1024B; Princeton Instruments). The signal-to-noise ratio was increased by 2 × 2 binning and 5 min exposure. For colocalization of the luminescent photon emission on the animal body, grey scale and pseudo-colour images were merged by using IMAGE-PRO PLUS (Media Cybernetics).

Antibiotics treatment. Antibiotics treatment was performed as previously described[20] using a combination of four antibiotics (4Abx) of ampicillin (1 g l^{-1}), neomycin (1 g l^{-1}), metronidazole (1 g l^{-1}) and vancomycin (500 mg l^{-1}), or vancomycin (500 mg l^{-1}) alone (VCM) in drinking water at the age of 13 weeks old until killed.

Histology and immunofluorescence analysis. Haematoxylin and eosin staining and immunofluorescence analysis were performed as previously described[16]. The primary antibodies used for mouse samples were as follows: α-SMA (Sigma A5228), desmin (abcam ab15200), p21 (abcam ab2961), p16 (Santa Cruz sc1207), 53BP1 (Santa Cruz sc22760), γ-H2AX (CST 9718), IL-6 (abcam ab6672), Gro-α (abcam ab17882), Ki-67 (Thermo RM9106), bromodeoxyuridine (abcam ab6326), caspase-1 (Millipore 06-503), IL-1β (R&D systems AF-401-NA), HSP47 (Santa Cruz sc8352), CXCL9 (abcam ab137792), F4/80 (Invitrogen BM8) and CD45(Millipore 05-1416). The primary antibodies used for human samples were as follows: α-SMA (Dako M0851), γ-H2AX (CST 9718), p16 (Santa Cruz sc56330), p21 (CST #2947), IL-6 (abcam ab6672), IL-8 (abcam ab18672), 53BP1 (Santa Cruz sc22760) and caspase-1 (Millipore 06-503).

Quantitative PCR. Total RNA was extracted from mouse tissues using TRIzol reagent (Life technologies) and reverse transcription and quantitative PCR were performed as previously described[22]. Primers used were as follows: human *GAPDH*, 5′-CAACTACATGGTTTACATGTTC-3′ (forward) and 5′-GCCAGTGGACT CCACGAC-3′ (reverse), mouse *Gapdh*, 5′-CAACTACATGGTCTACATGTTC-3′ (forward) and 5′-CACCAGTAGACTCCACGAC-3′ (reverse), human *IL-6*, 5′-CTCGACGGCATCTCAGCCCTGA-3′ (forward) and 5′-CTGCCAGTGCCTC TTTGCTGCTTT-3′ (reverse), mouse *Il-6*, 5′-TGATTGTATGAACAACGATG ATGC-3′ (forward) and 5′-GGACTCTGGCTTTGTCTTTCTTGT-3′ (reverse), human *IL-8*, 5′-AAGGAAAACTGGGTGCAGAG-3′ (forward) and 5′-ATTGC ATCTGGCAACCCTAC-3′ (reverse), mouse *Gro-α*, 5′-GCTGGGATTCACC TCAAGAA-3′ (forward) and 5′-AGGTGCCATCAGAGCAGTCT-3′ (reverse), bacterial *baiJ* 5′-TCAGGACGTGGAGGCGATCCA-3′ (forward) and 5′-TACRTGATACTGGTAGCTCCA-3′ (reverse), *Clostridium* cluster XI 16S rRNA gene 5′-TGACGGTACYYNRKGAGGAAGCC-3′ (forward) and 5′-ACT ACGGTTRAGCCGTAGCCTTT-3′ (reverse).

***In vivo* RNAi experiment.** 250 μl of siRNA solution (3 mg ml^{-1}) against HSP47 or control siRNA were mixed with 250 μl of complexation buffer and 500 μl of Invivofectamine (Life Technologies), incubated for 30 min at 50 °C, and dialysed at room temperature for 2 h in 1 l of PBS (pH 7.4). Dialysed siRNA-Invivofectamine complex was collected and 3 μg per g (weight) was injected through mice's tail vein twice a week for 15 weeks until killed. The sequences of HSP47 targeting oligo are as follows. 5′-GCACUGCUUGUGAACGCCAU GUUCU-3′ (sense), 5′-AGAACAUGGCGUUCACAAGCAGUGC-3′ (antisense). As a negative control, Ambion *In vivo* Negative Control #1 siRNA(4457289) was used.

Treatment with DCA, UDCA and DFAIII. Deoxycholic acid (DCA) was dissolved in absolute ethanol and diluted in 66% propylene glycol to reduce the concentration of alcohol to 5%. HFD-fed mice treated with DMBA at neonatal stage were fed a combination of four antibiotics (4Abx) with 40 μg per g (weight) of DCA or vehicle (control) three times per week using a plastic feeding tube at the age of 13 weeks old until killed. Ursodeoxycholic acid (UDCA) tablets (Tanabe-Mitsubishi Pharma) were powdered and dissolved in 66% propylene glycol. HFD-fed mice treated with DMBA at neonatal stage were fed 60 μg per g (weight) of UDCA or vehicle (control) using a plastic feeding tube every day at the age of 15 weeks old until killed. Difructose anhydride III (DFAIII)was dissolved in saline. HFD-fed mice treated with DMBA at neonatal stage were fed 0.1 mg per g (weight) of DFAIII or vehicle (control) using a plastic feeding tube every day at the age of 17 weeks old until killed.

Bacterial 16S rRNA amplicon sequencing and analysis. Bacterial genomic DNA was isolated from faeces using a QIAamp DNA Stool mini kit (QIAGEN), and 100 ng of DNA was used for PCR for V1–V4 hyper variable regions of the 16S rRNA gene. Twenty five cycles of amplification was performed with universal 16S rRNA primers 27F 5′-AGAGTTTGATCCTGGCTCAG-3′ and 519R 5′-GWATTACCGCGGCKGCTG-3′ with 10-bp barcode tags using KOD Fx plus DNA polymerase (TOYOBO). All amplicons were sequenced on a 454 Genome Sequencer FLX Titanium platform (Roche Diagnostics and Beckman Coulter Genomics). Quality filter-passed sequence reads were obtained by removing reads that had no both primer sequences, had less than 500 bp in length, had the average quality value (QV) < 25, or were possible chimaeric. Of the filter-passed reads, more than 2,500 sequence reads trimming off both primer sequences for each sample were used and subjected to OTU analysis with the cutoff similarity of 97% identity using QIIME software. Representative sequences from each OTU were blasted to the database in Ribosomal Database Project (RDP) and aligned. The obtained OTU sequences were grouped at class level[34,35] and were subjected to phylogenetic analysis using MEGA software as described previously[35].

Determination of the copy number of faecal bacteria. The copy number of faecal bacteria was calculated from the standard curve of known bacterial copy number by quantitative real-time PCR of 16S rRNA gene using 341f, 5′-CCTACGGGAGGC AGCAG-3′ and 534r 5′-ATTACCGCGGCTGCTGG-3′ primers as described previously[36].

Measurement of serum ALT and AST. The levels of serum alanine aminotransferase (ALT) and aspartate aminotransferase (AST) were measured using kits from WAKO Pure Chemical Industries, Ltd.

Measurement of serum deoxycholic acid. The metabolomic analysis of mice serum were performed by liquid chromatograph mass spectrometry(LC-MS) in Human Metabolome Technologies Inc. Japan as previously described[37]. The amount of serum DCA was measured by gas chromatograph mass spectrometry (GC-MS) in the Bile Acid Institute of Junshin Clinic, Japan as described[38].

Human subjects. Informed consent was obtained from all patients according to the protocol approved by the ethics committee of the Japanese Foundation for Cancer Research (JFCR).

Statistical analysis. Data were analysed by unpaired *t*-test with Welch correction (two-side) or Mann–Whitney test (two-side). *P*- values less than 0.05 were considered significant.

Cell culture. Murine primary HSCs were isolated as previously described[18,39], and were cultured in Dulbecco's modified Eagle's medium supplemented with 10% fetal bovine serum in 3% O_2 and 5% CO_2 condition. Human primary HSCs were purchased from Health Science Research Resources Bank and were grown in Dulbecco's modified Eagle's medium supplemented with 10% fetal bovine serum in 3% O_2 and 5% CO_2 condition.

***H-ras* sequencing.** Total RNA was prepared from HCCs and HSCs isolated from tumour regions using TRIzol reagent (Invitrogen). RNA was converted to cDNA by using oligo (dT) primer and a 330-bp PCR fragment containing exon 2 of *H-ras* gene was amplified with 5′-TGGGGCAGGAGCTCCTGGAT-3′ and 5′-GAA GGACTTGGTGTTGTTGA-3′ primers. PCR fragments were sub-cloned using Target Clone Plus system (TOYOBO) and were sequenced by using Dye-Terminator and Big-Dye cycle sequencing system (Applied Biosystems) as described previously[33].

31. Horai, R. *et al.* Production of mice deficient in genes for interleukin (IL)-1α, IL-1β, IL-1α/β, and IL-1 receptor antagonist shows that IL-1β is crucial in turpentine-induced fever development and glucocorticoid secretion. *J. Exp. Med.* **187,** 1463–1475 (1998).
32. Reagan-Shaw, S., Nihal, M. & Ahmad, N. Dose translation from animal to human studies revisited. *FASEB J.* **22,** 659–661 (2008).
33. Yamakoshi, K. *et al.* Real-time *in vivo* imaging of $p16^{Ink4a}$ reveals cross talk with p53. *J. Cell Biol.* **186,** 393–407 (2009).
34. Collins, M. D. *et al.* The phylogeny of the genus *Clostridium*: proposal of five new general and eleven new species combinations. *Int. J. Syst. Bacteriol.* **44,** 812–826 (1994).
35. Atarashi, K. *et al.* Induction of colonic regulatory T cells by indigenous *Clostridium* species. *Science* **331,** 337–341 (2011).
36. Song, Y., Liu, C. & Finegold, S. M. Real-time PCR quantitation of clostridia in feces of autistic children. *Appl. Environ. Microbiol.* **70,** 6459–6465 (2004).
37. Ooga, T. *et al.* Metabolomic anatomy of an animal model revealing homeostatic imbalances in dyslipidaemia. *Mol. Biosyst.* **7,** 1217–1223 (2011).
38. Muto, A. *et al.* Detection of Δ^4-3-oxo-steroid 5β-reductase deficiency by LC–ESI-MS/MS measurement of urinary bile acids. *J. Chromatogr. B* **900,** 24–31 (2012).
39. Sekiya, Y. *et al.* Down-regulation of cyclin E1 expression by microRNA-195 accounts for interferon-β-induced inhibition of hepatic stellate cell proliferation. *J. Cell. Physiol.* **226,** 2535–2542 (2011).

CORRIGENDUM

doi:10.1038/nature13004

Corrigendum: Obesity-induced gut microbial metabolite promotes liver cancer through senescence secretome

Shin Yoshimoto, Tze Mun Loo, Koji Atarashi, Hiroaki Kanda, Seidai Sato, Seiichi Oyadomari, Yoichiro Iwakura, Kenshiro Oshima, Hidetoshi Morita, Masahira Hattori, Kenya Honda, Yuichi Ishikawa, Eiji Hara & Naoko Ohtani

Nature **499,** 97–101 (2013); doi:10.1038/nature12347

In this Letter, the forename of author Masahira Hattori was spelled incorrectly as 'Masahisa'. It has been corrected in the HTML and PDF versions of the manuscript.

Miyanaga et al. BMC Cancer 2013, 13:262
http://www.biomedcentral.com/1471-2407/13/262

BMC Cancer

CASE REPORT Open Access

Activity of EGFR-tyrosine kinase and ALK inhibitors for *EML4–ALK*-rearranged non-small-cell lung cancer harbored coexisting *EGFR* mutation

Akihiko Miyanaga[1], Kumi Shimizu[1], Rintaro Noro[1], Masahiro Seike[1], Kazuhiro Kitamura[1], Seiji Kosaihira[1], Yuji Minegishi[1], Takehito Shukuya[7], Akinobu Yoshimura[1,8], Masashi Kawamoto[2,3], Shinichi Tsuchiya[2], Koichi Hagiwara[4], Manabu Soda[5], Kengo Takeuchi[6], Nobuyuki Yamamoto[7], Hiroyuki Mano[5], Yuichi Ishikawa[6] and Akihiko Gemma[1*]

Abstract

Background: The *EML4–ALK* (echinoderm microtubule-associated protein-like 4 gene and the anaplastic lymphoma kinase gene) fusion oncogene represents a novel molecular target in a small subset of non–small–cell lung cancers (NSCLCs). The *EML4–ALK* fusion gene occurs generally in NSCLC without mutations in epidermal growth factor receptor *(EGFR)* and *KRAS*.

Case presentation: We report that a case of *EML4–ALK*-positive NSCLC with *EGFR* mutation had a response of stable disease to both an EGFR tyrosine kinase inhibitor (EGFR-TKI) and ALK inhibitor.

Conclusions: We described the first clinical report of a patient with *EML4–ALK*-positive NSCLC with *EGFR* mutation that had a response of stable disease to both single-agent EGFR-TKI and ALK inhibitor. *EML4–ALK* translocation may be associated with resistance to EGFR-TKI, and EGFR signaling may contribute to resistance to ALK inhibitor in *EML4–ALK*-positive NSCLC.

Keywords: EML4–ALK, *EGFR* mutation, Lung cancer

Background

The *EML4–ALK* (echinoderm microtubule-associated protein-like 4 gene and the anaplastic lymphoma kinase gene) fusion oncogene was recently identified as a novel genetic alteration in non-small-cell lung cancer (NSCLC) [1]. *EML4–ALK* fusions have been detected in 2 to 7% of NSCLC patients. Patients harboring *ALK* rearrangements tend to be never and light smokers, have a history of adenocarcinoma, and be younger in age [1-6]. In general, the *EML4–ALK* fusion oncogene existed exclusively in NSCLC patients without the epidermal growth factor receptor (*EGFR*) gene mutation [1,7,8].

ALK inhibitors such as crizotinib are clinically effective in NSCLC patients harboring ALK rearrangements [9]. Crizotinib produced a high response rate and prolonged median progression-free survival among patients with ALK-positive NSCLC [9]. Crizotinib was recently approved by the US Food and Drug Administration and Japanese Ministry of Health, Labour and Welfare for the treatment of patients with advanced, ALK-rearranged NSCLC.

In this paper, we report a patient with NSCLC with concomitant ALK rearrangement and *EGFR* mutation that had a response of stable disease to both an EGFR tyrosine kinase inhibitor (EGFR-TKI) and ALK inhibitor.

Case presentation

In December 2009, a 55-year-old female who had never smoked was noted to have left lung opacity on a routine chest X-ray. No significant previous medical history was reported. Computed tomography (CT) scan of the chest revealed a 1.5 × 1.5 cm nodular lesion in the left upper lobe and hilar lymph node metastasis. Transthoracic needle biopsy histology revealed adenocarcinoma, and the histopathological subtype of the specimen was

* Correspondence: agemma@nms.ac.jp
[1]Department of Pulmonary Medicine and Oncology, Graduate School of Medicine, Nippon Medical School, Tokyo, Japan
Full list of author information is available at the end of the article

papillary adenocarcinoma with signet-ring cell components (Figure 1A-1C). The specimen was positive for periodic acid–Schiff (PAS) (Figure 1C). On immunohistochemical staining, the tumor cells were positive for thyroid transcription factor-1 (TTF-1) (Figure 1D). Laboratory findings were within normal range, except for the carcinoembryonic antigen (CEA) level of 158.0 ng/mL (normal range, 0 to 4.3 ng/mL) in the serum. She had multiple dorsal vertebra metastases (cT1N1M1b, stage IV).

Analysis for *EGFR* gene mutation was performed using a cytological specimen by means of the peptide nucleic acid–locked nucleic acid (PNA-LNA) polymerase-chain-reaction (PCR) clamp method as described previously [10,11]. The specimen showed a deletion in exon 19 (L747-A750del T751S). We collected mRNA from the same tumor specimens using Pinpoint Slide RNA Isolation System in order to clarify whether there was *EML4–ALK* (echinoderm microtubule-associated protein-like 4 gene and the anaplastic lymphoma kinase gene) fusion gene in each tumor. Reverse transcription polymerase-chain-reaction (RT-PCR) followed by direct sequencing confirmed the presence of *EML4–ALK* variant 2 [1] (Figure 2). In addition, *EML4–ALK* was identified by using fluorescent in situ hybridization (FISH) for *ALK* rearrangements (Figure 3B) and was confirmed by immunohistochemistry for ALK expression in tumor [2] (Figure 3A).

A platinum doublet was chosen as first line therapy according to existing treatment protocol in 2009. Four cycles of combination chemotherapy comprising cisplatin and pemetrexed was administered at 3-week intervals. She was judged as having a stable disease. After 7 months, spinal magnetic resonance imaging (MRI) revealed progression of the dorsal vertebra lesions. Therefore, EGFR-TKI was chosen as a 2nd-line therapy. She received gefitinib therapy at 250 mg/day administered orally for 2 months. CT imaging of the chest showed that the pulmonary nodule was not growing after gefitinib therapy, and the tumor marker levels had not changed. However, spinal MRI demonstrated growing dorsal vertebra metastases 2 months after the start of gefitinib therapy. The carcinoembryonic antigen (CEA) level increased from 117 ng/ml to 250 ng/ml. Therefore, the patient was judged as having progressive disease. After local radiation therapy with a total of 30 Gy for dorsal metastases, a second EGFR-TKI was chosen given the stable primary disease. She received another EGFR-TKI, erlotinib (150 mg/day), as 3rd-line therapy. After being progression-free for 3 months, spinal MRI revealed a growing thoracic vertebra metastasis. She received 4th-line treatment with 2 cycles of docetaxel (DTX). However, her disease progressed 6 months later. Finally, she received a targeted inhibitor of ALK. The patient initially had SD associated with a temporary decrease in the CEA level from 743 ng/ml to 520 ng/ml, but her disease progressed after 4 months of therapy. The ALK inhibitor treatment was

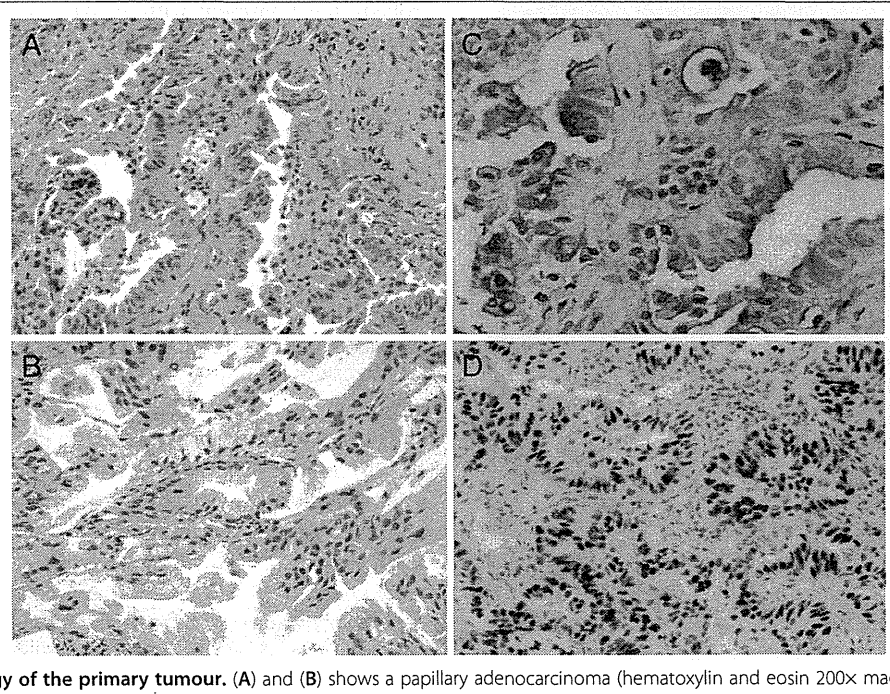

Figure 1 Histology of the primary tumour. (**A**) and (**B**) shows a papillary adenocarcinoma (hematoxylin and eosin 200× magnification), (**C**) a mucin stain shows positive for both signet-ring and papillary morphology (PAS, 400× magnification). **(D)** immunohistochemical analysis of lung adenocarcinoma specimens with *EML4-ALK* fusion using a monoclonal anti-TTF-1 antibody (200× magnification).

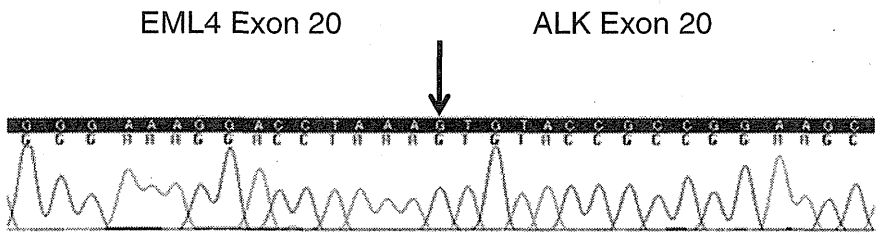

Figure 2 The sequence of the junction between *EML4* exon 20 and *ALK* exon 20.

ceased and full supportive care was given. All lines of therapy were well tolerated.

Discussion

We presented a patient with NSCLC with concomitant ALK rearrangement and *EGFR* mutation that had a response of stable disease to both EGFR-TKI and ALK inhibitors. The presence of *EML4–ALK* generally seems to be mutually exclusive of the presence of *EGFR* or *KRAS* mutations in NSCLC [1,7,8]. Previous reports showed twelve cases of *EML4–ALK*-positive lung cancer with *EGFR* mutation [3,12-17]. Only one patient with harboring *ALK* translocation and EGFR mutation was treated by ALK inhibitor has been reported [17]. Lee et al. reported two ALK-positive and EGFR-mutant NSCLC patient who did not respond to EGFR-TKI but achieved a durable partial response to ALK inhibitor [17]. The present patient was a woman with no history of smoking. Her pathological diagnosis was papillary adenocarcinoma with a signet-ring cell component, which was consistent with the previously reported characteristics of *EML4–ALK*-positive lung adenocarcinoma except for the *EGFR* mutation status [1-6]. It was reported that EGFR-TKI therapy among patients with advanced NSCLC and *EGFR* mutations revealed a response rate of more than 60% and progression-free survival of 9 to 14 months [11,18,19]. In addition, recent reports showed that ALK inhibition in NSCLC patients with the *ALK* rearrangement resulted in tumor shrinkage or stable disease in most patients [9]. Unfortunately, EGFR-TKI treatment was not effective in the tumor regression nor tumor marker level of present patient (disease might be controlled), but treatment with an ALK inhibitor resulted in SD with decreasing tumor markers. Therefore, this case showed that ALK rearrangement might be superior to EGFR mutation for the driver mutation.

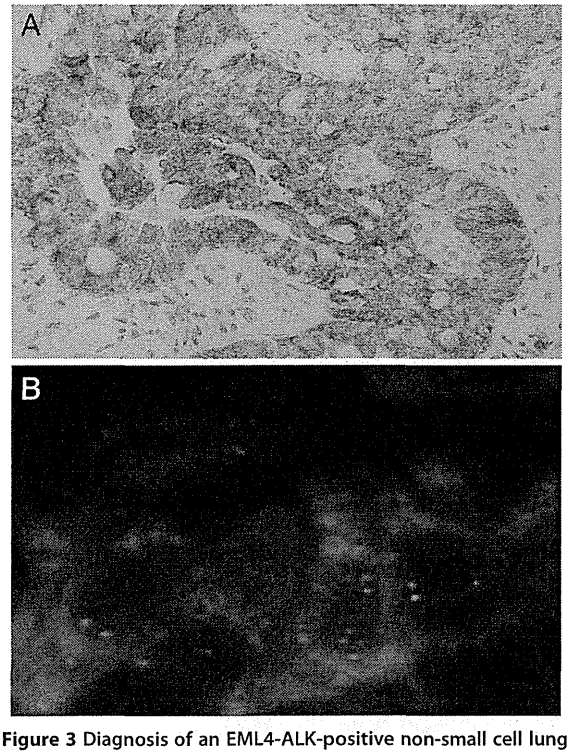

Figure 3 Diagnosis of an EML4-ALK-positive non-small cell lung cancer. (**A**) Immunostaining for ALK protein expression in tumor cells. (**B**) The results of a break-apart FISH assay of tumor cells from a patient with rearrangement of the gene encoding *ALK*.

It was reported that *EML4–ALK* fusion was associated with resistance to EGFR-TKIs [20]. Patients with NSCLC in the *EML4–ALK* cohort and the wild type cohort showed similar response rates to platinum-based combination chemotherapy and no difference in overall survival [20]. Whereas *EGFR* mutations confer sensitivity to EGFR-TKIs, *EML4–ALK* is strongly associated with resistance to EGFR-TKIs. In a previous case of concomitant *EGFR* mutation and *ALK* translocation, the patient presented the most durable response to an EGFR-TKI and was a case demonstrating no EML4–ALK expression by immunohistochemistry with an *EML4–ALK* rearrangement characterized by an isolated 3_ FISH signal [12]. Our patient presented a concurrent *EML4-ALK* rearrangement and ALK expression by immunohistochemistry; however, EGFR-TKI was not effective.

Among patients with both *EML4–ALK* rearrangement and *EGFR* mutation, *in vitro* studies showed that EGFR signaling can contribute to ALK inhibitor resistance in EML4–ALK NSCLC [14]. In addition, these findings suggested that a cancer cell line that harbors a concurrent

ALK rearrangement and an *EGFR* mutation would be expected to be resistant to both single agent ALK and EGFR inhibitors [14]. We suggest that the combination of both ALK and EGFR inhibitors as early-line treatment may represent an effective therapy for this subset of NSCLC patients.

Conclusions

This is the first clinical report of a patient with *EML4–ALK*-positive NSCLC with *EGFR* mutation that had a response of stable disease to both single-agent EGFR-TKI and ALK inhibitor. The *EML4–ALK* fusion gene defines a new molecular subset of NSCLCs with distinct clinical and pathologic features. NSCLCs with *ALK* rearrangement are highly sensitive to ALK inhibition. However, EGFR signaling may contribute to ALK inhibitor resistance in *EML4–ALK* NSCLC. Therefore, we suggest that this provides a translational opportunity whereby laboratory studies should be undertaken to understand the biological link between ALK rearrangement and *EGFR* mutation, with a view to establishing whether there is preclinical justification for using combination therapy for NSCLC with concomitant ALK rearrangement and *EGFR* mutation.

Consent

Written informed consent was obtained from the patient for publication of this case report and accompanying images.

Abbreviations

EML4: Echinoderm microtubule-associated protein-like 4; ALK: Anaplastic lymphoma kinase; NSCLC: Non-small cell lung cancer; EGFR: Epidermal growth factor receptor; TKI: Tyrosine kinase inhibitor; CT: Computed tomography; PAS: periodic acid–Schiff; TTF-1: Thyroid transcription factor-1; PNA-LNA: Peptide nucleic acid–locked nucleic acid; PCR: Polymerase chain reaction technique; FISH: Fluorescent in situ hybridization; SD: Stable disease; MRI: Magnetic resonance imaging (MRI); CEA: Carcinoembryonic antigen; RT-PCR: Reverse transcription polymerase chain reaction.

Competing interests

The authors declare that they have no competing interests.

Authors' contributions

AM prepared the manuscript and the literature search; RN and MS reviewed and edited the manuscript; HM and AG corrected and revised the manuscript; KS, KK, SK, YM, MS and TS treated and observed the patient; MK and ST performed the histopathological, immunohistochemical examinations; and AY, KH, KT, NY and YI reviewed the manuscript. All authors read and approved of the final manuscript.

Acknowledgements

The authors wish to thank Mari Masuda for technical support in the sequence alignment.

Author details

[1]Department of Pulmonary Medicine and Oncology, Graduate School of Medicine, Nippon Medical School, Tokyo, Japan. [2]Division of Diagnostic Pathology, Nippon Medical School Hospital, Tokyo, Japan. [3]Department of Clinical Pathology, University Hospital, Mizonokuchi, Teikyo University School of Medicine, Kanagawa, Japan. [4]Saitama Medical School Respiratory Organs Internal Medicine, Saitama, Japan. [5]Division of Functional Genomics, Jichi Medical University, Tochigi, Japan. [6]Division of Pathology, The Cancer Institute, Japanese Foundation for Cancer Research, Tokyo, Japan. [7]Division of Thoracic Oncology, Shizuoka Cancer Center, Shizuoka, Japan. [8]Department of Clinical Oncology, Tokyo Medical University Hospital, Tokyo, Japan.

Received: 17 January 2013 Accepted: 22 May 2013
Published: 29 May 2013

References

1. Soda M, Choi YL, Enomoto M, Takada S, Yamashita Y, Ishikawa S, Fujiwara S, Watanabe H, Kurashina K, Hatanaka H, *et al*: **Identification of the transforming EML4-ALK fusion gene in non-small-cell lung cancer.** *Nature* 2007, **448**(7153):561–566.
2. Takeuchi K, Choi YL, Soda M, Inamura K, Togashi Y, Hatano S, Enomoto M, Takada S, Yamashita Y, Satoh Y, *et al*: **Multiplex reverse transcription-PCR screening for EML4-ALK fusion transcripts.** *Clin Can Res* 2008, **14**(20):6618–6624.
3. Koivunen JP, Mermel C, Zejnullahu K, Murphy C, Lifshits E, Holmes AJ, Choi HG, Kim J, Chiang D, Thomas R, *et al*: **EML4-ALK fusion gene and efficacy of an ALK kinase inhibitor in lung cancer.** *Clin Can Res* 2008, **14**(13):4275–4283.
4. Mano H: **Non-solid oncogenes in solid tumors: EML4-ALK fusion genes in lung cancer.** *Cancer Sci* 2008, **99**(12):2349–2355.
5. Wong DW, Leung EL, So KK, Tam IY, Sihoe AD, Cheng LC, Ho KK, Au JS, Chung LP, Pik Wong M: **The EML4-ALK fusion gene is involved in various histologic types of lung cancers from nonsmokers with wild-type EGFR and KRAS.** *Cancer* 2009, **115**(8):1723–1733.
6. Perner S, Wagner PL, Demichelis F, Mehra R, Lafargue CJ, Moss BJ, Arbogast S, Soltermann A, Weder W, Giordano TJ, *et al*: **EML4-ALK fusion lung cancer: a rare acquired event.** *Neoplasia* 2008, **10**(3):298–302.
7. Inamura K, Takeuchi K, Togashi Y, Nomura K, Ninomiya H, Okui M, Satoh Y, Okumura S, Nakagawa K, Soda M, *et al*: **EML4-ALK fusion is linked to histological characteristics in a subset of lung cancers.** *J Thorac Oncol* 2008, **3**(1):13–17.
8. Shinmura K, Kageyama S, Tao H, Bunai T, Suzuki M, Kamo T, Takamochi K, Suzuki K, Tanahashi M, Niwa H, *et al*: **EML4-ALK fusion transcripts, but no NPM-, TPM3-, CLTC-, ATIC-, or TFG-ALK fusion transcripts, in non-small cell lung carcinomas.** *Lung Cancer* 2008, **61**(2):163–169.
9. Kwak EL, Bang YJ, Camidge DR, Shaw AT, Solomon B, Maki RG, Ou SH, Dezube BJ, Janne PA, Costa DB, *et al*: **Anaplastic lymphoma kinase inhibition in non-small-cell lung cancer.** *N Engl J Med* 2010, **363**(18):1693–1703.
10. Nagai Y, Miyazawa H, Huqun, Tanaka T, Udagawa K, Kato M, Fukuyama S, Yokote A, Kobayashi K, Kanazawa M, *et al*: **Genetic heterogeneity of the epidermal growth factor receptor in non-small cell lung cancer cell lines revealed by a rapid and sensitive detection system, the peptide nucleic acid-locked nucleic acid PCR clamp.** *Cancer Res* 2005, **65**(16):7276–7282.
11. Maemondo M, Inoue A, Kobayashi K, Sugawara S, Oizumi S, Isobe H, Gemma A, Harada M, Yoshizawa H, Kinoshita I, *et al*: **Gefitinib or chemotherapy for non-small-cell lung cancer with mutated EGFR.** *N Engl J Med* 2010, **362**(25):2380–2388.
12. Popat S, Vieira de Araujo A, Min T, Swansbury J, Dainton M, Wotherspoon A, Lim E, Nicholson AG, O'Brien ME: **Lung adenocarcinoma with concurrent exon 19 EGFR mutation and ALK rearrangement responding to erlotinib.** *J Thorac Oncol* 2011, **6**(11):1962–1963.
13. Tiseo M, Gelsomino F, Boggiani D, Bortesi B, Bartolotti M, Bozzetti C, Sammarelli G, Thai E, Ardizzoni A: **EGFR and EML4-ALK gene mutations in NSCLC: a case report of erlotinib-resistant patient with both concomitant mutations.** *Lung Cancer* 2011, **71**(2):241–243.
14. Sasaki T, Koivunen J, Ogino A, Yanàgita M, Nikiforow S, Zheng W, Lathan C, Marcoux JP, Du J, Okuda K, *et al*: **A novel ALK secondary mutation and EGFR signaling cause resistance to ALK kinase inhibitors.** *Cancer Res* 2011, **71**(18):6051–6060.
15. Tanaka H, Hayashi A, Morimoto T, Taima K, Tanaka Y, Shimada M, Kurose A, Takanashi S, Okumura K: **A case of lung adenocarcinoma harboring EGFR mutation and EML4-ALK fusion gene.** *BMC Cancer* 2012, **12**(1):558.
16. Kuo YW, Wu SG, Ho CC, Shih JY: **Good response to gefitinib in lung adenocarcinoma harboring coexisting EML4-ALK fusion gene and EGFR mutation.** *J Thorac Oncol* 2010, **5**(12):2039–2040.
17. Lee JK, Kim TM, Koh Y, Lee SH, Kim DW, Jeon YK, Chung DH, Yang SC, Kim YT, Kim YW, *et al*: **Differential sensitivities to tyrosine kinase inhibitors in NSCLC harboring EGFR mutation and ALK translocation.** *Lung Cancer* 2012, **77**(2):460–463.

18. Fukuoka M, Wu YL, Thongprasert S, Sunpaweravong P, Leong SS, Sriuranpong V, Chao TY, Nakagawa K, Chu DT, Saijo N, *et al*: Biomarker analyses and final overall survival results from a phase III, randomized, open-label, first-line study of gefitinib versus carboplatin/paclitaxel in clinically selected patients with advanced non-small-cell lung cancer in Asia (IPASS). *J Clin Oncol* 2011, 29(21):2866–2874.
19. Mitsudomi T, Morita S, Yatabe Y, Negoro S, Okamoto I, Tsurutani J, Seto T, Satouchi M, Tada H, Hirashima T, *et al*: Gefitinib versus cisplatin plus docetaxel in patients with non-small-cell lung cancer harbouring mutations of the epidermal growth factor receptor (WJTOG3405): an open label, randomised phase 3 trial. *Lancet Oncol* 2010, 11(2):121–128.
20. Shaw AT, Yeap BY, Mino-Kenudson M, Digumarthy SR, Costa DB, Heist RS, Solomon B, Stubbs H, Admane S, McDermott U, *et al*: Clinical features and outcome of patients with non-small-cell lung cancer who harbor EML4-ALK. *J Clin Oncol* 2009, 27(26):4247–4253.

doi:10.1186/1471-2407-13-262
Cite this article as: Miyanaga *et al.*: Activity of EGFR-tyrosine kinase and ALK inhibitors for *EML4–ALK*-rearranged non–small–cell lung cancer harbored coexisting *EGFR* mutation. *BMC Cancer* 2013 13:262.

Human Pathology (2014) 45, 1045–1056

ELSEVIER

Human PATHOLOGY

www.elsevier.com/locate/humpath

Original contribution

A subset of small cell lung cancer with low neuroendocrine expression and good prognosis: a comparison study of surgical and inoperable cases with biopsy☆,☆☆,★

Wakako Hamanaka MD, PhD[a,b], Noriko Motoi MD, PhD[a], Shumpei Ishikawa MD, PhD[c], Masaru Ushijima PhD[d], Kentaro Inamura MD, PhD[a], Satoko Hatano[a], Hirofumi Uehara MD, PhD[e], Sakae Okumura MD[e], Ken Nakagawa MD[e], Makoto Nishio MD, PhD[f], Takeshi Horai MD, PhD[f], Hiroyuki Aburatani MD, PhD[c], Masaaki Matsuura PhD[d], Akinori Iwasaki MD, PhD[b], Yuichi Ishikawa MD, PhD[a,*]

[a]*Division of Pathology, The Cancer Institute, The Cancer Institute Hospital, Japanese Foundation for Cancer Research (JFCR), Tokyo 135-8550, Japan*
[b]*Department of Thoracic Surgery, Fukuoka University School of Medicine, Fukuoka 814-0180, Japan*
[c]*Genome Science Division, Research Center for Advanced Science and Technology, The University of Tokyo, Tokyo 153-0041, Japan*
[d]*Genome Center, The Cancer Institute Hospital, Japanese Foundation for Cancer Research (JFCR), Tokyo 135-8550, Japan*
[e]*Division of Respiratory Surgery, The Cancer Institute Hospital, Japanese Foundation for Cancer Research (JFCR), Tokyo 135-8550, Japan*
[f]*Division of Respiratory Medicine, Thoracic Oncology Center, The Cancer Institute Hospital, Japanese Foundation for Cancer Research (JFCR), Tokyo 135-8550, Japan*

Received 20 July 2013; revised 27 December 2013; accepted 2 January 2014

Keywords:
Small cell lung cancer (SCLC);
Prognosis;
Neuroendocrine;
Basal cell;
Immunohistochemistry

Summary Patients with small cell lung carcinoma (SCLC) rarely demonstrate long-term survival. We previously reported that gene expression profiling identified a subset of SCLC with good prognosis in surgical cases. To find an easier way to routinely identify SCLC belonging to this subset, we conducted the present study with a hypothesis that neuroendocrine (NE) or basaloid (BA) phenotypes may influence prognosis. To confirm the subset, we used an array platform to analyze fresh samples. Because inoperable cases may differ from surgical cases, we enrolled 51 biopsy cases and 43 resected samples. To evaluate NE and BA phenotypes, we used NE (synaptophysin, chromogranin A, and CD56) and BA (p63 and CK34βE12) markers. To varying extents, expression profiling based on the array platform

☆☆ Competing interests: The authors have no potential conflicts of interest.

★ Funding/Support: This work was supported by Grants-in-Aid for Scientific Research from the Ministry of Education, Culture, Sports, Science and Technology and from the Japan Society for the Promotion of Science, and grants from the Ministry of Health, Labour and Welfare, the Smoking Research Foundation, and the Japan Science Technology Agency.

* Corresponding author. Yuichi Ishikawa, MD, PhD, Division of Pathology, The Cancer Institute, JFCR, 3-8-31 Ariake, Koto-ku, Tokyo 135-8550, Japan.
E-mail addresses: ishikawa@jfcr.or.jp (Y. Ishikawa).

0046-8177/$ – see front matter
http://dx.doi.org/10.1016/j.humpath.2014.01.001

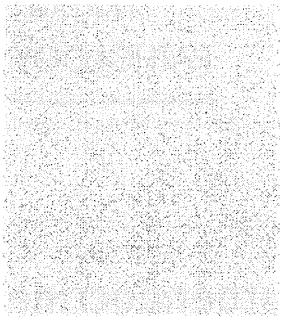

duplicated the subsets. For NE phenotypes, 77% of surgical cases and 100% of biopsy cases were positive for at least 1 marker. For BA phenotypes, only 19% of surgical cases were positive for at least 1 marker, whereas there were no positive biopsy cases. Cases undergoing surgery were categorized based on NE and BA immunoreactivity; 58% into NE+BA−, 19% into NE+BA+, 23% into NE−BA−, and 0 into NE−BA+ groups. NE− patients (n = 10) demonstrated a significantly better prognosis (P = .0306) than their NE+ counterparts (n = 33), whereas no survival difference was evident between the BA+ and BA− groups. Multivariate analyses showed that NE positivity was an independent prognostic factor. In conclusion, the SCLC subset with good prognosis is identified by low NE marker expression, which was found only in surgical cases.

1. Introduction

Small cell lung carcinoma (SCLC) accounts for about 15% of all lung cancers, and its high proliferative activity generally leads to early metastasis to lymph nodes and distant organs. It is known that, although more sensitive to chemotherapy and irradiation than non-SCLCs [1,5], SCLCs tend to recur in about 70% of cases [6]. Some cases that are initially misdiagnosed are only found to be SCLC after resection [7]. Including these cases, it has been found that stage I SCLC has only a 42% to 66% 5-year survival, which is much lower than for non-SCLCs [8,9]. These statistics reflect a disparate course, with some patients with SCLC surviving for a long time after therapy, whereas others appear insensitive to chemotherapy and irradiation, implying considerable heterogeneity.

SCLC has distinct histologic characteristics such as scant cytoplasm (high nucleocytoplasmic [N/C] ratio), ill-defined cell borders, finely granular nuclear chromatin, absent or inconspicuous nucleoli, round to spindle shaped, nuclear molding and rosette formation, extensive necrosis, and a high mitotic rate [10]. Surgically resected tumors show somewhat different histology such as larger cell sizes, occasional conspicuous nucleoli, and vesicular nuclear chromatin [7]. It is necessary to prove neuroendocrine (NE) differentiation by immunohistochemistry (IHC) or electron microscopy for the diagnosis of large cell NE carcinoma (LCNEC). However, according to the World Health Organization (WHO) classification [10], this is not mandatory for SCLC. Nevertheless, without IHC, it is sometimes difficult to differentiate an SCLC from a poorly differentiated non-SCLC composed of small-sized cells with a high N/C ratio, such as basaloid (BA) carcinoma. In such cases, immunohistochemical markers for BA cells are useful in distinguishing NE carcinomas from poorly differentiated squamous cell carcinomas and BA carcinomas [11,12]. It is important to distinguish such carcinomas from SCLC because they may have a better prognosis than SCLC, although BA carcinoma has a poorer prognosis than usual squamous cell carcinomas.

We previously identified a subset of SCLC with good prognosis by global gene expression profiling using custom-made complementary DNA (cDNA) microarrays [13], showing that differentially expressed genes included NE-related genes, implying that long-term survival is not simply a matter of chance. To further characterize this subset and define a more readily accessible technique, such as IHC, to identify this subset, we set out this study by hypothesizing that a degree of NE differentiation or a basal cell nature may be related to prognosis. Because this subset had been delineated in surgically resected cases and inoperable cases may possibly differ from surgical cases, we also enrolled inoperable cases using available biopsy materials. First, we confirmed the existence of the subset using another platform of gene expression profiling and then performed IHC with NE and basal cell markers for surgical and biopsied cases. We paid particular attention to excluding atypical carcinoids.

2. Materials and methods

2.1. Patients and tumor samples

Surgical samples of SCLC are scarce: during the period from January 1990 to December 2004, a total of 1568 lung cancers were resected surgically at the Cancer Institute Hospital, Japanese Foundation for Cancer Research, Tokyo, Japan. Among these cancers, only 56 cases (3.6%) were found to be SCLC by pathological examination of resected materials. In this study, we enrolled a total of 96 SCLC cases, which were composed of 45 surgical cases and 51 inoperable cases with only biopsy specimens available. Histologic diagnosis of SCLC was made according to the 2004 WHO classification [10], relying only on hematoxylin and eosin (H&E) staining. Cases with atypical histology were examined by a panel of Japanese expert pathologists organized by an NE tumor study group [9], supported by the Ministry of Health, Labour and Welfare. Also, a few of the atypical cases were presented at the Pathology Committee meeting of the International Association for the Study of Lung Cancer, held in Tokyo, Japan. Atypical carcinoids were carefully excluded, with special attention to mitosis and cell morphology. Excluding some SCLC cases with extensive degeneration due to induction therapy, or with insufficient tumor cells remaining after chemotherapy, 45 surgical tumors were used for this

analysis. Among these, fresh materials for 30 tumors were suitable for microarray gene expression analysis (18 were previously examined [13] and 12 were newly enrolled in this study), and for the remaining 15 cases, only paraffin blocks were available. Because for 2 cases among the 30, only fresh materials were available, no paraffin tissues from surgical materials being left for this study, tissues of 43 cases were used for immunohistochemical studies. In addition to the surgical cases, 51 patients who were inoperable and had undergone a biopsy between 1996 and 2006 were enrolled.

All tumors were pathologically staged according to the TNM classification system of the International Union Against Cancer [14] using resected materials. The clinical stages, serum level of markers (NSE, ProGRP, CEA, SCC, and CYFRA), and response rates to chemotherapy were investigated using medical records. Cumulative smoking was carefully surveyed and described with reference to the *smoking index* (SI), defined as the product of the number of cigarettes per day and duration in years. Cause of death was surveyed thoroughly using death certificates, and lung cancer–specific survival or overall survival was analyzed as appropriate. All tissues were collected with informed consent from patients, and the study protocol was approved by the Japanese Foundation for Cancer Research institutional review board.

2.2. RNA isolation and gene expression profiling

Fresh samples of 30 SCLCs were obtained at surgery. The tissues of resected tumors were grossly dissected and snap-frozen in liquid nitrogen typically within 15 minutes of removal. We always confirmed that fresh tumor tissues for RNA extraction actually contained viable SCLC cells, using frozen section diagnosis. Total RNA was extracted using an RNeasy Mini kit (Qiagen, Hilden, Germany) according to the manufacturer's instructions. A 3-μg aliquot was used to generate ds-cDNA using a T7-Oligo (dT) primer, and the cDNA was transcribed into biotin-labeled cRNA using a GeneChip 3′ IVT Express Kit (Affymetrix, Santa Clara, CA, USA). Quality control of RNA and cRNA was performed using a bioanalyzer (Agilent Technologies, Santa Clara, CA, USA). After fragmentation, each sample was hybridized to Affymetrix HG U133 plus 2.0, which covers 38 500 genes, 47 400 transcripts, and more than 54 000 probe sets, and was stained according to the manufacturer's instructions (Affymetrix). We used GeneChip Scanner 3000 for scanning and GeneChip Operating Software (GCOS; Affymetrix) for data output.

2.3. Array data analysis

Data were analyzed and visualized by use of R software (version 2.9.2; www.t-project.org). Before analysis, all data were log transformed and subjected to Robust Multichip Average normalization [15].

Unsupervised hierarchical clustering analysis was accomplished with standard Pearson correlations and the Ward method using 15 530 probe sets expressed above the background in at least 20% of the 30 samples and 100 or more expression signals. To identify genes that represent the most informative markers between 2 groups obtained from clustering analysis about SCLC, we focused on those with $P < .01$ by the Welch t test and log fold-change above 2.0 or below −2.0.

2.4. Procedures for tumor tissue arrays

Surgical specimens were fixed with 15% buffered formalin and embedded in paraffin. They were sectioned at 4-μm thickness and stained with H&E for histologic diagnosis. Tissue arrays were made from paraffin specimens as follows: 2 spots of the most representative tumor area were selected considering heterogeneity and cored in 2-mm diameter with a tissue-arraying instrument (Azumaya, Tokyo, Japan). In cases of combined SCLC, only SCLC components were chosen for coring. Core samples were retrieved from donor tissues and arrayed in a new paraffin block.

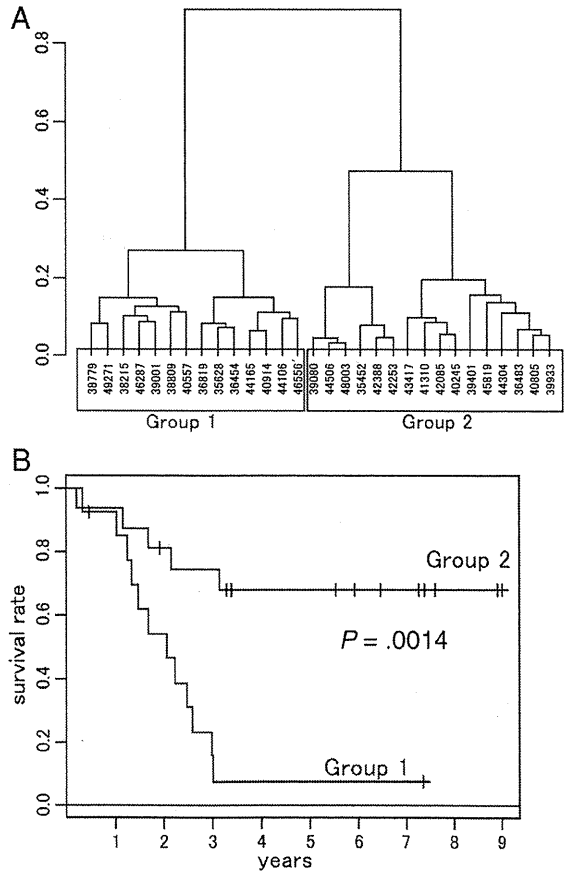

Fig. 1 A, Results of unsupervised hierarchical clustering of 30 SCLCs. B, SCLC-specific survival of groups 1 and 2. Note the better survival of group 2 as compared with group 1 ($P = .0014$).

Table 1 Patients characteristics of resected SCLC and LCNEC

Cases	Ref. no.	Diagnosis	Age (y)	Sex	SI	cT	cN	cM	Preoperative diagnosis	Induction chemotherapy (reduction rate)		Operation	pT	pN
1	29635	SCLC	76	M	1500	2	2	0	SCLC	Yes	PR: 84%	Lobectomy	4	2
2	30017	SCLC	57	M	1050	4	2	0	SCLC	Yes	PR: 70%	Lobectomy	4	2
3	30156	SCLC	67	M	940	3	2	0	SCLC or LCC	None		Lobectomy	4	2
4	30323	SCLC	59	M	1435	2	1	0	SCLC	Yes	CR: scar+	Lobectomy	2	2
5	30865	SCLC	64	M	400	1	0	0	p/d ca	None		Lobectomy	1	2
6	31160	SCLC	68	M	1000	1	0	0	SCLC	None		Lobectomy	4	0
7	31401	SCLC	72	M	680	1	0	0	SCLC	None		Lobectomy	2	0
8	32658	SCLC	84	M	1200	1	0	0	Unconfirmed	None		Partial resection	1	1
9	33130	SCLC	46	M	940	1	0	0	SCLC or SQ	None		Lobectomy	2	0
10	33587	Combined SCLC + AD	59	M	1480	1	1	0	AD or LCC	None		Lobectomy	4	0
11	34802	SCLC	73	M	960	1	0	0	SQ	None		Lobectomy	1	0
12	34947	SCLC	54	M	680	1	0	0	SCLC	Yes	PR: 74%	Lobectomy	1	0
13	35452	Combined SCLC + AD		F	0	2	0	0	AD	None		Lobectomy	2	0
14	35628	SCLC	73	M	800	1	2	0	AD or SCLC	Yes	PR: 77%	Lobectomy	1	0
15	35996	SCLC	61	M	375	1	2	0	SCLC	Yes	PR: 79%	Lobectomy	4	2
16	36454	SCLC	66	M	300	1	1	0	SCLC	Yes	SD: 24%	Lobectomy	1	1
17	36483	Combined SCLC + Spindle	64	M	1470	3	0	0	SCLC	Yes	PR: 67%	Lobectomy	4	0
18	36819	SCLC	67	M	920	2	2	0	SCLC	Yes	CR: regrowth+	Lobectomy	1	2
19	38779	SCLC	57	M	1110	1	0	0	SCLC	Yes	SD: 26%	Lobectomy	1	1
20	38809	SCLC	79	M	1180	2	0	0	SCLC	None		Lobectomy	4	0
21	39001	Combined SCLC + AD	59	M	675	1	0	0	SCLC	None		Lobectomy	1	0
22	39080	SCLC	76	M	600	1	0	0	AD or SCLC	None		Segmentectomy	1	0
23	39401	SCLC[c]	67	M	2000	1	2	0	Unconfirmed	None		Partial resection	1	0
24	39933	SCLC	53	M	1050	2	1	0	SCLC	None		Pneumonectomy	4	2
25	40557	Combined SCLC + AS	74	F	0	2	1	0	NSCLC	None		Lobectomy	2	2
26	40805	SCLC	68	M	1440	2	0	0	p/d ca	None		Lobectomy	2	0
27	40914	SCLC	68	F	380	2	0	0	AD or SCLC	None		Lobectomy	4	1
28	41179	SCLC	65	M	2400	2	1	0	SCLC	Yes	PR: 51.3%	Lobectomy	4	1
29	41310	SCLC	64	F	700	1	0	0	carcinoma	None		Lobectomy	1	0
30	42085	SCLC	71	M	1060	1	0	0	SCLC or p/d ca	None		Lobectomy	1	1
31	42253	Combined SCLC + LCNEC	63	F	1880	3	0	0	SQ or SCLC	None		Lobectomy	4	0
32	43417	SCLC	74	M	200	2	1	0	NEC	None		Lobectomy	2	0
33	44106	SCLC	62	M	1175	1	0	0	SCLC	Yes	PR: 69.5%	Lobectomy	1	1
34	44165	Combined SCLC + LCC	70	M	1000	1	0	0	SCLC or LCC	None		Lobectomy	2	0
35	44304	Combined SCLC + LCC	63	M	3760	2	0	0	SCLC	None		Lobectomy	4	0
36	45819	SCLC	70	F	1000	2	0	0	SCLC	Yes	SD: 25.2%	Lobectomy	2	0
37	46287	SCLC	68	F	160	2	0	0	SCLC	Yes	PR: 73%	Lobectomy	4	0
38	49271	Combined SCLC + AD	80	M	840	2	0	0	AD	None		Lobectomy	2	2
39	50455	SCLC	70	M	1000	1	0	0	SCLC	None		Lobectomy	1	0
40	40245	SCLC	63	M	1660	2	0	0	SCLC	Yes	PR: 52.6%	Lobectomy	2	0
41	42388	Combined SCLC + AD	74	F	0	1	0	0	AD	No		Lobectomy	1	1
42	44506	SCLC	56	M	780	1	0	0	SCLC	Yes	PR: 50%	Lobectomy	1	0
43	48003	SCLC	68	F	270	1	0	0	SCLC	Yes	PR: 47%	Lobectomy	1	0

Table 1 (*continued*)

pM	p-Stage	Size (mm)	p	pm	v	ly	Adj-CTx	Reccurence	Treatment for recurrence: Regimen	Treatment for recurrence: Reduction status	Prognosis	Final follow-up (d)	Cause of death	Group
0	IIIB	22	1	1	1	1	Yes	Yes	CTx	PR	Dead	296	Pneumonia	N+B−
1	IV	50	0	2	1	0	Yes	Yes	CRTx	SD	Dead	737	Lung cancer	N+B+
0	IIIB	70	3	0	1	1	Yes	Yes	CTx	SD	Dead	568	Lung cancer	N+B+
0	IIIA	32	0	0	1	1	Yes	Yes	CRTx	CR	Dead	616	Lung cancer	N+B−
0	IIIA	16	0	0	0	1	Yes	None			Dead	732	Unknown	N+B−
0	IIIB	18	0	1	1	1	Yes	None			Alive	5825		N−B−
0	IB	33	0	0	1	0	Yes	Yes	Unknown[a]		Dead	617	Lung cancer	N+B+
0	IIA	20	2	0	1	1	None	Yes	Unknown[a]		Dead	209	Lung cancer	N+B−
0	IB	33	0	0	1	0	Yes	None			Alive	4103		N+B−
0	IIIB	26	0	1	1	1	None	None			Alive	4029		N+B−
0	IA	24	0	0	1	0	None	None			Dead	495	Mesentric embolism	N+B+
0	IA	22	0	0	1	0	Yes	Yes	CRTx + Op	PD	Dead	747	Lung cancer	N+B−
0	IB	45	0	0	1	0	Yes	None			Dead	2691	Unknown	N+B−
0	IA	20	1	0	1	0	None	None			Dead	174	Pneumonia	N+B−
0	IIIB	13	0	0	1	1	Yes	None			Alive	4072		N+B+
0	IIA	16	0	0	1	1	Yes	Yes	CTx	PD	Dead	373	Lung cancer	N+B−
0	IIIB	42	3	0	1	0	Yes	Yes	Unknown[a]		Dead	616	Lung cancer	N+B−
0	IIIA	25	0	0	1	1	Yes	Yes	CTx	PD	Dead	465	Lung cancer	N+B+
0	IIA	22	0	0	1	0	Yes	Yes	RTx	PR	Dead	948	Lung cancer	N+B−
0	IIIB	40	1-3[b]	1	1	1	None	Yes	RTx	CR	Dead	1098	Lung cancer	N+B−
0	IA	20	0	0	1	1	Yes	None			Alive	2682		N+B−
0	IA	19	0	0	1	0	None	Yes	CTx	SD	Dead	1157	Lung cancer	N+B−
0	IA	15	0	0	0	0	Yes	None			Alive	2167		N−B−
0	IIIB	58	3 (interlobe)	0	1	1	None	Yes	None[d]		Dead	77	Lung cancer	N−B−
0	IIIA	54	0	0	1	1	None	Yes	RTx	PD	Dead	120	Lung cancer	N+B+
0	IB	49	0	0	1	1	Yes	None			Alive	2623		N−B−
0	IIIB	48	1	1	1	1	Yes	Yes	RTx	CR	Dead	815	Lung cancer	N+B−
0	IIIB	11	0	1	1	1	None	None			Dead	312	Lung cancer	N+B−
0	IA	30	0	0	0	0	Yes	None			Dead	702	Respiratory failure	N−B−
0	IIA	20	0	0	1	1	Yes	None			Alive	3077		N−B−
0	IIIB	80	3	0	1	0	Yes	None			Alive	3037		N−B−
0	IB	80	1	0	1	0	Yes	None			Alive	2772		N−B−
0	IIA	15	2	0	1	1	Yes	Yes	CRTx	PR	Dead	1094	Lung cancer	N+B−
0	IIB	23	2	0	1	0	None	Yes	None[e]		Dead	620	Lung cancer	N+B−
0	IIIB	21	0	1	1	1	Yes	None			Alive	2363		N+B+
0	IB	32	1-3[b]	0	1	1	Yes	None			Dead	1203	Unknown	N+B−
0	IIIB	53	3	0	1	1	None	Yes	CRTx	PR	Dead	538	Lung cancer	N+B−
0	IIIA	31	0	0	1	0	Yes	Yes	Unknown[a]		Dead	760	Lung cancer	N+B−
0	IA	22	0	0	1	0	Yes	None			Alive	1330		N+B−
0	IB	32	1	0	0	1	Yes	None			Dead	1239	Other cancer	N−B−
0	IIA	30	0	0	1	1	No	Yes	RTx	SD	Dead	432	Lung cancer	N−B−
0	IA	9	0	0	0	0	No	Yes	RTx	PR	Dead	792	Lung cancer	N+B−
0	IA	11	0	0	0	0	No	None			Alive	2025		N+B−